STARS

Electronic Theses and Dissertations, 2004-2019

2010

Thermal Detection Of Biomarkers Using Phase Change Nanoparticles

Chaoming Wang
University of Central Florida

Part of the Materials Science and Engineering Commons

Find similar works at: https://stars.library.ucf.edu/etd

University of Central Florida Libraries http://library.ucf.edu

Showcase of Text, Archives, Research & Scholarship

THERMAL DETECTION OF BIOMARKERS USING PHASE CHANGE

NANOPARTICLES

by

CHAOMING WANG
B.S, Chemical Engineering and Technology, 2004, Hubei University
M.S, Materials Chemistry, 2007, Chinese Academy of Sciences

A thesis submitted in partial fulfillment of the requirements
for the degree of Master of Materials Science and Engineering
in the Department of Mechanical, Materials and Aerospace Engineering
in the College of Engineering and Computer Science
at the University of Central Florida
Orlando, Florida

Summer Term
2010

ABSTRACT

Most of existing techniques cannot be used to detect molecular biomarkers (i.e., protein and DNA) contained in complex body fluids due to issues such as enzyme inhibition or signal interference. This thesis describes a nanoparticle-based thermal detection method for the highly sensitive detections of multiple DNA biomarkers or proteins contained in different type of fluids such as buffer solution, cell lysate and milk by using solid-liquid phase change nanoparticles as thermal barcodes. Besides, this method has also been applied for thrombin detection by using RNA aptamer-functionalized phase change nanoparticles as thermal probes. Furthermore, using nanostructured Si surface that have higher specific area can enhance the detection sensitivity by four times compared to use flat aluminum surfaces. The detection is based on the principle that the temperature of solid will not rise above its melting temperature unless all solid is molten, thus nanoparticles will have sharp melting peak during a linear thermal scan process. A one-to-one correspondence can be created between one type of nanoparticles and one type of biomarker, and multiple biomarkers can be detected simultaneously using different type nanoparticles. The melting temperature and the heat flow reflect the type and the concentration of biomarker, respectively. The melting temperatures of nanoparticles are designed to be over 100°C to avoid interference from species contained in fluids. The use of thermal nanoparticles allows detection of multiple low concentration DNAs or proteins in a complex fluid such as cell lysate regardless of the color, salt concentration, and conductivity of the sample.

Dedicated to

My parents, wife and families

ACKNOWLEDGEMENTS

TABLE OF CONTENTS

LIST OF FIGURES

CHAPTER 1: INTRODUCTION

1.1 Cancer detection using biomarkers

Cancer is the result of genetic instability and accumulation of multiple molecular alterations.[1] Cancer can occur in all races. According to National Vital Statistics Reports (2002-2006), among 100,000 persons, the numbers of cancer patients were 470.6 in White people, 493.6 in Black people, 311.1 in Asians, and 350.6 in Hispanics, Among all forms of cancers, lung cancer, breast cancer and prostate cancer are three leading causes of death in the United States, claiming over 227,900 lives in 2007 alone. It has been found that if cancer could be diagnosed at early stage and remains in the primary site, the five-year survival rate can increase significantly. Unfortunately, not many cancers can be detected at early stage based on current diagnostic techniques, and by the time when cancers are identified, significant spreading of the cancer to other organ systems has occurred.

Normally people with pre-cancer symptoms such as unidentified bleeding will be asked to take physical examinations such as computer tomography, X-ray, magnetic resonance imaging (MRI) and biopsy.[2-4] But, unless a large solid tumor is present, the diagnostic outcomes strongly depend on the sensitivity of the method to detect cancer from the general tissue background, and in most cases results have a high false positive rate. Traditional X-ray scan has a low resolution and cannot identify cancers smaller than millimeters. Even with spiral computed tomography, which is the most accurate technique available, bronchial cancers at early stage cannot be detected. Computer tomography strongly depends on contrast agents to enhance image quality, has low sensitivity, and agents themselves could have adverse effects on patients. Biopsy has

been used for cancer detection, but the invasive nature of the process is painful for patient, and small cancer may also not be detected. Another method to visualize lung cancer is to use fiberoptic bronchoscopy, but it cannot be used for screening purpose due to its invasive nature; meanwhile, such method can only identify large cancer tumors in main airways.[5]

The multistage growth of cancers is characterized by gradual accumulation of molecular abnormalities, resulting in uncontrolled growth of cells. Such genetic abnormalities are involved in a wide range of cell dynamics including cell cycles, senescence, apoptosis, cellular repair, differentiation and migration. Recent advances in molecular biology have opened up many new opportunities for the detection and diagnosis of cancer using genetic abnormalities or proteins as biomarkers. Principally, it is possible to detect cancer earlier than current methods by detecting cancer-related genes or proteins, before the appearance of observable abnormality at cell level. However, a significant challenge is to turn this rich molecular biology knowledge into advances in diagnosis. The main reason is that cancer genetic biomarkers are not effective, even in the case of widely used prostate specific antigen (PSA).[6] Meanwhile, these abnormal genes or proteins almost always have very low concentration in a biologically diverse environment. The difference between normal and cancer genes may be only base pair. In the case of protein, the concentration of cancer-specific antigen may be too low and have a large protein background. Detecting a low concentration DNA or protein of not-so-effective biomarkers under a huge background will be a great challenge, will be very expensive for most of current techniques such as polymerase chain reaction, and is not economically favorable for early screening.[7] In order to establish an effective cancer detection strategy, it would be appropriate to create a highly sensitive miniaturized device which requires small amount of sample. Furthermore, it is desirable that multiple biomarkers can

be detected to enhance detection reliability for reliable detection and screening at an early stage. Such detections will leave sufficient time for effective treatment of cancer at an operable stage.

1.2 Existing methods of in vitro cancer biomarker detection

Biosensors have been attracting much attention and extensively studied over the last two decades for diseases diagnostics and detection of biological molecules. Traditional biosensing methods normally used for cancer biomarker detection include polymerase chain reaction (PCR), enzyme-linked immunosorbent assay (ELISA), and DNA microarray.[8-10] These approaches have certain advantages such as high-throughput, and the ability for amplification, but these methods cannot detect ultralow concentration of biomarkers, cannot perform readout in body fluids, and need extensive sample preparation efforts.

1.2.1 Polymerase chain reaction

Polymerase chain reaction (PCR) was developed in 1983, and is a technique in molecular biology to amplify a single or few copies of a piece of DNA segment by several orders of magnitude, generating thousands to millions of copies of a particular DNA sequence. PCR is an indispensable technique in medical and biological research labs for a variety of applications.[11, 12] It allows early diagnosis of fatal diseases, such as leukemia and lymphomas, with high sensitivity and identification of non-cultivatable or slow-growing microorganisms, such as mycobacteria, anaerobic bacteria, or viruses. Besides, PCR assays can be carried out directly on genomic DNA samples to detect translocation in specific malignant cells. The PCR diagnosis is based on the detection of infectious agents and the discrimination of non-pathogenic from pathogenic strains by specific genes. In the case of PCR based viral DNA detection, the primers used are specific to

the target viral DNA sequences. The high sensitivity of PCR permits virus detection soon after infection and before onset of disease, which gives physicians a significant lead in treatment. PCR approach can detect all organisms regardless of physiological state and is fast and easy to perform. However, PCR method has a big limitation: it is easy to pick up contaminants.

1.2.2 Enzyme-linked immunosorbent assay

Enzyme-linked immunosorbent assay (ELISA) has been used for detecting the presence and concentration of a particular antibody or antigen in a fluid sample. The test procedure is as follows (Figure 1.1): (1) prepare a surface and bind a known quantity of primary antibody to it; (2) apply the antigen-containing sample to the surface; (3) apply secondary antibody that also binds specifically to the antigen; (4) apply enzyme linked secondary antibody that binds to the secondary antibody; (5) apply a chemical that is converted by the linked enzyme into a colored product. The concentration of the colored product is measured by a spectrophotometer and the intensity of color is proportional to the concentration of bound antigen. ELISA test is very convenient, can detect antigens with low or unknown concentrations, and has high specificity since the capture antibody only captures the specific antigen. In addition, it does not require radioactive substances and can be used in a wide variety of tests. However, ELISA test has some major drawbacks: the secondary antibody must recognize the primary antibody; negative controls may indicate positive results if blocking solution is ineffective, because secondary antibody or antigen can bind to open sites as well; enzyme/substrate reaction is short term so that microwells must be read as soon as possible.
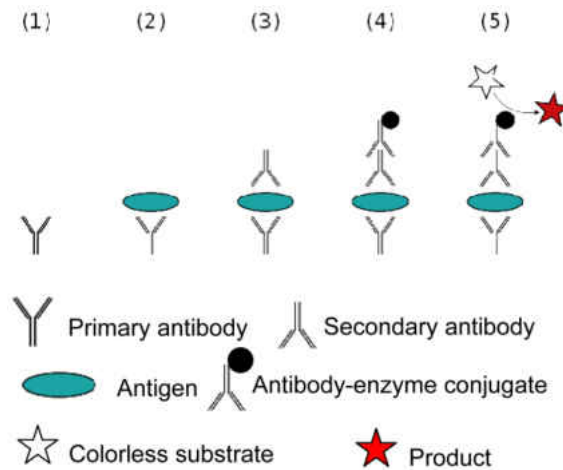
Figure 1.1 Scheme of a sandwich ELISA test.

1.2.3 DNA microarray

A DNA microarray is a collection of microscopic DNA spots attached to a solid surface. It consists of an arrayed series of microscopic spots of DNA oligonucleotides, and each spot contains picomoles (10^{-12} moles) of a specific DNA sequence known as probes. A short section of a gene or other DNA segments is used as probes to hybridize a targeted complementary DNA or RNA sample under high-stringency conditions. Probe-target hybridization is usually detected and quantified by fluorescence-based detection of fluorescently labeled targets to determine relative abundance of nucleic acid sequences. Since a DNA microarray contains thousands of probes, one experiment can accomplish many genetic tests at the same time. Therefore using DNA microarrays have dramatically accelerated many types of investigation. DNA microarrays can be used to express large numbers of genes simultaneously, find new biomarkers, and detect DNA, RNA, proteins, cancer biomarkers, etc.[13-15] Although the DNA microarray is very useful in medical diagnostics and biodetection, it have some limitations: it is relatively expensive; it is

not readily or easily reproducible; the data quantity often overwhelms the users and make the analysis and interpretation is difficult; for this fluorescence based detections, the dyes molecules tend to photo-bleach after certain time, which decreases the lifetime or measurement time.

1.3 Nanomaterials for cancer biomarker detection

The advent of nanostructured materials and micro-fabricated devices enables the construction of highly sensitive, ultra-small, and portable sensing devices with multiple detection capability. As sizes of the sensing elements in these devices are reduced to nanometer, unique optical, electrical or electrochemical, and magnetic properties of the nanomaterials allow them to be used for more selective, sensitive and precise detection of biomarkers. Nanomaterials have become an effective tool for biodetection due to the following reasons: (1) their small size allows intimate contact with biomolecules, (2) surface properties can be modified to efficiently capture target molecules, (3) detection signal can be amplified by physical means; (4) size, surface, composition and morphology of the nanoparticles can be tuned precisely.

1.3.1 Biosensing using nanoparticles

The presence of biomarkers in the sample will cause nanoparticles to be immobilized onto a substrate or combine with another nanoparticle; a physical signal transduction method can be used to derive the existence and concentration of target biomarkers. The nanoparticle based biosensing can be performed in three-stranded configuration for DNA detection or sandwiched configuration for protein detection (Figure 1.2). For DNA detection using three-stranded configuration, the surface of nanoparticles is first modified with probe DNA that can bind to one end of target DNA, and a substrate is modified with capture DNA that can bind to the other end

of the target DNA. The solid substrate is immersed into the solution containing target DNA, after hybridization, the substrate is washed and then immersed into a solution containing probe DNA functionalized nanoparticles. The target DNA will immobilize nanoparticles onto the substrate through DNA hybridization. The immobilized nanoparticles are then readout by using a physical method to reflect the existence and concentration of the target DNA.
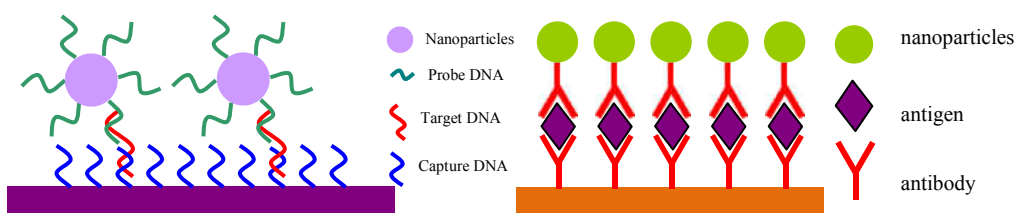
Figure 1.2 Nanoparticles based three-stranded (left) and sandwiched (right) configuration for DNA and protein detection, respectively.

Similarly, for protein detection using a sandwiched configuration, a substrate is modified with primary antibody that can capture the target antigen, and the surface of nanoparticles is modified with secondary antibody that can bind to the target antigen. After immersing into a solution containing the target antigen, the substrate is then incubated with secondary antibody functionalized nanoparticles and the nanoparticles are immobilized onto the substrate surface by antibody-antigen-antibody interaction. The signal from the immobilized nanoparticles measured by a physical method will indicate the existence and concentration of the target antigen.

1.3.2 Surface modification

A variety of strategies have been used to modify surfaces of nanoparticles or substrates. The most widely used sensing surfaces are gold, glass, indium tin oxide (ITO), carbon and

silicon. Gold thin films or nanoparticles can be modified with self-assembled monolayer of alkanethiols. Thiol molecules can form gold-sulfur complex bond, and form highly ordered monolayer on gold surfaces through self-assembly. Different terminated functional groups can be used to conjugate biological recognition elements. For example, carboxyl groups are used to immobilize antibody; esters for amine couplings; biotin coupling can be used to bind streptavidin and further biotin functionalized biomolecules. Silanes with methoxy or ethoxy residues have been used to modify glass or silicon surfaces by reacting with surface hydroxyls, and the other end of silane molecule provides a reactive residue to bind to biomolecules. For example, in order to immobilize antibody on glass surface, 3-amino-propyltrimethoxysilane (APTES) can be used to ammonize the substrate, which is followed by activating surface with a bifunctional cross-linker-disuccinimidyl suberate (DSS), and the other end of the cross-linker will be conjugated to the free amine group of antibody (Figure 1.3).
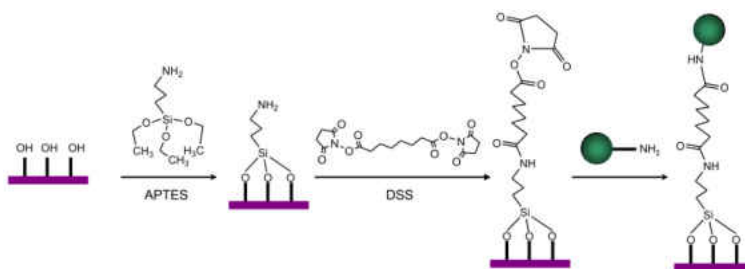
Figure 1.3 Immobilizing antibody on a glass substrate by surface chemistry.

1.3.3 Fluorescence nanoparticles

Semiconductor nanoparticles made by colloid chemistry methods have shown fluorescent emissions in visible light range, and the wavelength can be controlled by changing composition

and size of nanoparticles. Semiconductor nanoparticles have been widely used in biological imaging and bioanalyses including cell staining, cell surface receptor targeting, DNA, protein and biomarkers detection.[16-20] The readout from fluorescent nanoparticles can be performed with a spectrophotometer to indicate the presence and concentration of target molecules. The detection can be done with three-stranded and sandwiched configurations by monitoring intensity of fluorescence light. Compared to traditional dyes that tend to photobleach, semiconductor nanoparticles exhibit important advantages in terms of high luminescence and photostablility.[21] Semiconductor nanoparticles can improve detection sensitivity due to their large surface to volume ratio. However, semiconductor nanoparticles suffer from a serious limitation for multiplexed detection. According to Rayleigh criterion on spectral resolution, if the distance between two peaks is shorter than their half width at maximal height, these two peaks will not be resolved from each other (Figure 1.4). Normally, complex peak resolving algorithm will have to be used. In the case of semiconductor nanoparticles, although individually, the emission peaks can be controlled to be sharp by precisely controlling their diameters, once nanoparticles of different colors are mixed, it will be difficult to resolve the spectrum. The peak width at half height of normal fluorescence semiconductor nanoparticles is about 150 nm. In the visible range from 400 to 900 nm, the maximum number of different nanoparticles that can be resolved would be about 4-5, meaning the detection multiplicity would be very low.
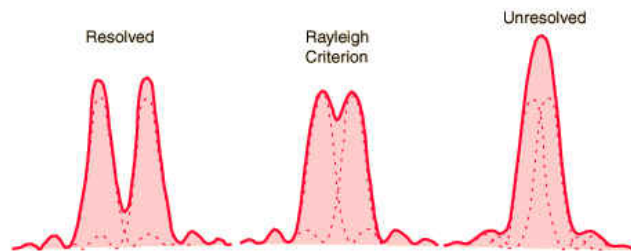
Figure 1.4 Rayleigh criterion.

1.3.4 Plasmonic nanoparticles

Surface plasmon resonance (SPR) biosensors, based on metallic nanoparticles, can be used for DNA, protein and cancer biomarker detection.[22-26] Surface plasmons are surface electromagnetic waves that propagate in a direction parallel to the metal/dielectric interface. Since the wave excited by light propagates on the boundary of the metal and the external medium (e.g., air or water), these oscillations are very sensitive to any changes that take place on the boundary, such as the adsorption of molecules to the boundary. For metallic nanoparticles, the wave is very sensitive to the changes in shape and size of the nanoparticles as well as the interparticle distance. These phenomenon form the basis of many standard tools for detecting the adsorption of molecules onto the surface of metallic nanoparticles and for determining the concentration of biomolecules through color changes induced by biological events or through surface plasmon resonance peak shift of the nanoparticles.

The SPR spectral profile and peak wavelength λ_{max} depend on the composition, size, shape and local dielectric environment of the nanoparticles. The simplest theoretical approach for modeling the optical properties of nanoparticles is the Mie theory, which is described as[27]

$$E(\lambda) = \frac{24\pi N_A a^3 \varepsilon_m^{3/2}}{\lambda \bullet \ln(10)} \left[\frac{\varepsilon_i}{(\varepsilon_r + \chi \varepsilon_m)^2 + \varepsilon_i^2} \right] \qquad (1)$$

$E(\lambda)$ is the extinction (sum of absorption and scattering), N_A is the density of nanoparticles, a is the radius of the metallic nanosphere, ε_m is the dielectric constant of the medium surrounding the metallic nanosphere, λ is the wavelength of the absorbing radiation, ε_i is the imaginary portion of the metallic nanoparticle's dielectric function, ε_r is the real portion of the metallic nanoparticle's dielectric function, and χ is the term that describes the aspect ratio of the nanoparticle (equal to 2 for a sphere). From the equation, it is clear that the SPR spectrum of an isolated metallic nanosphere embedded in an external dielectric medium will depend on the nanoparticle radius a, composition of the nanoparticles (ε_i and ε_r), and the environment's dielectric constant (ε_m). The peak wavelength λ_{max} occurs when the denominator of the term in brackets approaches zero. This occurs at the wavelength where ε_i is small and $\varepsilon_r = -\chi \varepsilon_m$. For spherical nanoparticles, χ is equal to 2 and the equation is modified such that the peak wavelength λ_{max} occurs when $\varepsilon_r = -2\varepsilon_m$. In order to study the surface plasmon response of nanoparticles due to changes in their dielectric environment, a technique that produces nanoparticles with uniform size and shape is required. However, achieving this is challenging for most scientific researchers. In addition to uniformity, it is also important to develop surface plasmon resonance sensors that are stable against solvent annealing. To overcome theses issues, nanoparticles can be pretreated in water or organic solvents. However, this will make the detection process time-consuming.

1.3.5 Electrochemical detection using nanostructured electrodes

Electrochemical biosensors have been used to detect nucleic acids, proteins, antibodies, cells or cancer biomarkers in body fluids, food samples, cell cultures and environmental samples due to their smart size and quick and dependable response compared to the conventional biodetection systems.[28-30] The detection mechanism is based on that the sensors convert the redox reactions occurring at electrode surfaces into electronic signals, which can be processed by a processing system and readout through an interface to the human operator. Nanostructured electrodes have been widely used to increase the electro-active surface area and enhance electron transfer due to their high surface-to-volume ratio, good biocompatibility, conductivity and catalytic properties. The increase in electro-active surface area allows for lower detection limit and higher sensitivity to analytes. Typically, nanostructured electrodes can be made by attaching metallic nanoparticles, or nanowire or nanotube arrays.[31-33]

Although nanostructured electrode surface can be made by the surface modification, capping reagents, cross-linker molecules, and other binder materials (e.g., polymer) will more or less affect the electron-transfer reactions. In order to avoid these issues, an alternative way should be developed to attach the nanoparticles onto the electrode surfaces without using a linker molecule or polymer to magnify the effective electrochemical responses and suppress the unfavorable effects. Various metallic nanoparticles can be attached to the electrode surfaces without using a linker molecule for electrochemical analysis by the seed-mediated growth or electrochemical deposition method. The attached nanoparticles can increase the electro-active surface area and adsorb more bridging molecules. Thus the electron transfer process is accelerated and the signal can be measured by the electrical equipment when the redox-activate

analyte bind with the bridging molecules. Although a low limit of detection can be obtained by this technique, the nanoparticles attached on the electrode surfaces are not very robust and the modified surfaces are difficult to be recovered once damaged.

Nanowires or nanotubes modified electrodes have been widely used in electrochemical biosensors for biological detection because of their high surface-to-volume ratio and good electron transport properties. Highly dense nanowires or nanotubes standing on the electrode surface can be synthesized efficiently by using a template through self-assembling process, electrochemical deposition, molecular beam epitaxy or electron beam evaporation.[34, 35] By controlling the experimental conditions (e.g., the template), the structure of the nanowires or nanotubes can be adjusted conveniently and their properties can be tuned effectively. It should be noticed that the wire or tube diameter, wire surface condition, crystal structure and its quality, chemical composition and crystallographic orientation along the wire axis are important parameters that influence the conductance of the nanowires. When the analytes are adsorbed onto the surface of the nanowires or nanotubes, which have been modified by a bridging molecule (e.g., enzyme), a significant electrical response is observed because of the redox reaction that took place on the surfaces. Although high sensitivity can be achieved by using the nanowires or nanotubes modified electrodes, the uniformity and the growth orientation still limit the wide use of electrochemical biosensors. Furthermore, after the detection process, the nanowires or nanotubes surface may form an oxide layer, which is not recoverable.

1.3.6 Magnetic nanoparticle for biodetection

Biosensing strategies based on magnetic nanoparticles have received considerable attention because they offer unique advantages over other techniques. For example, magnetic

nanoparticles are inexpensive to produce, physically and chemically stable, biocompatible, and environmentally safe. In addition, biological samples exhibit virtually no magnetic background, and thus highly sensitive measurements can be performed in turbid or otherwise visually obscured samples without any further processing. To date, numerous methods using magnetic labels have been developed to detect biomolecules. These techniques use magnetometers, such as superconducting quantum interference device sensors, giant magnetoresistive (GMR) sensors, and Hall sensors, to directly detect magnetic nanoparticles and derive the concentration of the target biomolecules.[36-38] In particular, GMR sensors have triggered scientific researchers' interest because it have shown great potentials for the detection of DNA, proteins, microorganisms, cancer biomarkers, etc.
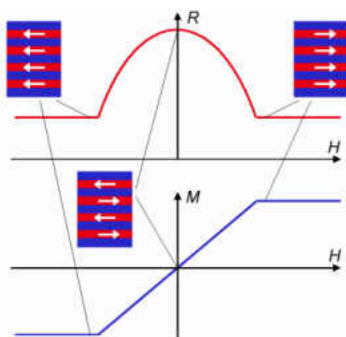
Figure 1.5 Schematic description of the giant magnetoresistance effect. Blue curve: magnetization of the multilayer versus applied magnetic field. Red curve: electrical resistance of the multilayer. The insets indicate the magnetic configuration of the multilayer in zero field and at positive and negative saturation fields.

GMR sensors are sensitive, can be easily integrated with electronics and microfluids, and can generate fully electronic signals. Giant magnetoresistance is a quantum mechanical magnetoresistance effect observed in thin film structures composed of alternating ferromagnetic

and non magnetic layers. Depending on whether the magnetization of adjacent ferromagnetic layers is in parallel or in antiparallel alignment, the electrical resistance of the thin film exhibits a significant difference. Namely, the overall resistance is relatively low for parallel alignment and relatively high for antiparallel alignment (Figure 1.5). GMR sensors are based on the binding of magnetic particles to a sensor surface where the magnetic fields of the particles alter the magnetic field of the sensor which results in changes in electrical current within the sensor. There are two mechanisms through which magnetic particles bind to the sensor surface: (i) direct labeling and (ii) indirect labeling (a sandwich type binding). Normally, magnetic probes bind to functionalized surfaces in direct labeling by using streptavidin-biotin interaction or complementary DNA sequence recognition (Figure 1.6). While indirect labeling uses a sandwich configuration. For example, primary antibodies that bind to the target protein are immobilized on the surface. After treatment of the surface with a sample solution containing the target proteins, biotinylated second antibodies are added to the system. Finally, streptavidin coated magnetic particles are applied for tagging the biotinylated antibodies. This magnetic biodetection system is based on detecting fringing field of captured magnetic nanoparticle labels for bimolecular detection. The significant advantage of GMR sensors is their high sensitivity to small changes in the magnetic fields. However, for all their advantages, the GMR sensors have one serious drawback because their manufacture requires a complicated technology. Besides, low reading signals arising at re-magnetization of magnetic nanoparticles is also one of the main problems at the design of GMR biosensors.
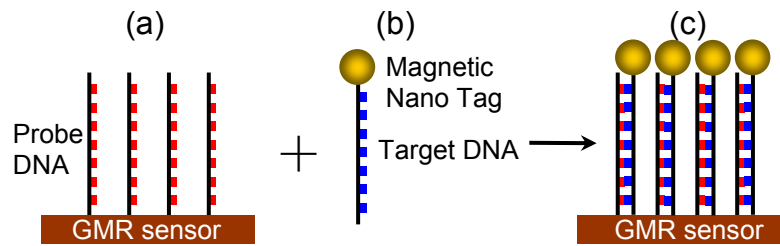
Figure 1.6 Principle of biosensor using magnetic and magnetic nanotags. The resistance of the sensor is altered by the magnetic field generated from attached nanoparticles.

1.3.7 Nanowire and nanotube for biodetection

One dimensional semiconductor nanomaterials, in particular silicon nanowires and carbon nanotubes have been used in biosensing. These nanomaterials have extremely high surface-to-volume ratio and sensitivity of the carrier mobility to the variations in the electric field (charge density) at their surface, make them ideal for field effect transistors (FETs) based biosensors for label-free, sensitive and real-time detection of biological objects.[39] The sensing mechanism of silicon nanowire or carbon nanotube FETs is based on the surface change in charge density that induces an electric field change at the silicon nanowire or carbon nanotube surface after some biological events have occurred, such as analyte adsorption, DNA hybridization or antibody-antigen binding. Theoretical calculations suggest that nanowire sensors have much shorter response time and this will make the real-time detection of biological molecules possible. In the real-time detection process, the conductance of an individual single-walled carbon nanotube (SWCNT), or a network of SWCNTs, during the introduction of the analyte solution, is monitored and the resistance of the device is found to be either directly or inversely proportional to the concentration of the analyte.

16

However, nanotube/nanowire based biosensors are difficult to produce. Normally, nanowire or nanotubes are made first by chemical vapor deposition method. The as made tangled bundles have to be separated and purified, and cut into appropriate lengths. Subsequently, they have to be deposited across electrodes to form stable connections. Although many techniques have been developed to manipulate nanowires using electrical field, microfluid, atomic force microscopy or dielectrophoresis, these methods have low yield, and take a lot of time.[40-43] Furthermore, even if nanowires could be aligned between electrodes, each nanowire should be modified with different species, which requires site-specific patterning tools, such as dip-pen nanolithography (DPN). After modification, each wire should be electrically connected out, and the readout circuit could be very complex if multiple species are to be detected.

1.3.8 Nano-mechanical cantilever for biosensing

Microcantilevers have been used to detect DNA and RNA, protein, glucose, and cardiac biomarkers by detecting changes in nanomechanical properties (bending or vibrating) induced by biological interactions.[44-49] The microcantilevers are normally made of silicon or silicon nitride using microfabrication techniques, and the normal dimensions of a microcantilever are $20 \times 40 \times 0.6$ μm^3. One side of cantilever is coated with thin films of gold to reflect laser beam, which is then directed into a position sensitive detector. The bending or vibration of cantilever can be monitored using laser optical levers with high precision. Cantilever bending can also be monitored using other techniques such as piezoelectric sensors, tunneling current and optical interferometry. Microcantilevers can be operated in two modes to detect biomolecules static mode and dynamic mode, where either the surface stress or the resonance frequency of the cantilever is measured (Figure 1.7).
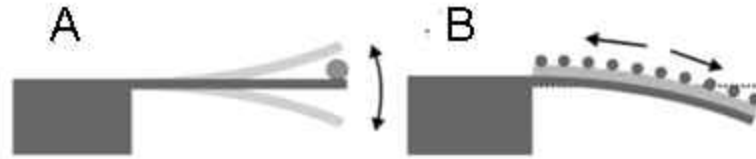
Figure 1.7 Cantilever sensor modes of operation: (A) dynamic mode and (B) static mode

In the dynamic mode, cantilevers are excited close to their resonance frequency typically in the kHz or even MHz range, and can be treated as an ideal oscillator with a basic resonance frequency of

$$f = \frac{1}{2\pi} \sqrt{\frac{k_{spring}}{m^*}} \tag{2}$$

where k_{spring} is the spring constant and m^* is an effective mass (taking into account the cantilever geometry and mass distribution along the cantilever). The attachment of target biomolecules on microcantilever leads to mass change, which in turn leads to frequency shift into the low frequency end. The sensitivity of mass detection depends strongly on the geometry of the microcantilevers. By engineering the geometry of the cantilever, single molecular mass change can also be detected using cantilever with high intrinsic frequency (stiffness). However, dynamic mode cannot be used in solution due to viscous damping, which broadens the resonant peak and reduces sensitivity of mass resolution. A recent and interesting development avoids damping by combining microfluid with microcantilever and delivering liquid in hollow cantilevers. This eliminates viscous damping and maintains mass sensitivity of cantilever sensors. But the cost of fabrication is too high due to high failure rate of production.

In the static mode, the asymmetric binding of target molecules on one side of cantilever will produce intermolecular stress and change surface stress of the cantilever leading to a bend of

the cantilever. Normally, the gold reflection film on cantilever is modified through gold-thiol chemistry, and the other side (silicon or silicon nitride) is coated with polymer to reduce non-specific binding. The surface stresses produced in cantilever can be described using Stoney's formula:

$$\Delta\sigma = \frac{Et^3}{3(1-v)L^2}\Delta z \qquad (3)$$

where $\Delta\sigma$ is the difference in surface stress between the bottom and top surfaces of a cantilever, E is elasticity modulus, v is the Poisson ratio (which is about 0.3 for silicon), t is the cantilever thickness, L is the cantilever length and Δz is the cantilever deflection. The cantilevers operating in static mode can be used to detect gas molecules, metal ions and biomolecules. But, asymmetric surface modification of cantilever is not easy to do; surface stress is extremely sensitive to uniformity of molecular coating, which can lead to sensitivity variation; the thermal energy from exothermic or endothermic surface reactions creates a resultant temperature change on the cantilever, resulting in unwanted heat induced bending, thereby, introducing erroneous results.

Most importantly, although multiple microcantilevers can be generated to detect multiple biomarkers at the same time, the readout electronics will be very complex and hard to achieve. Although multiple micro-mirrors have been designed to overcome this issue, it is found that each cantilever will have different response due to thickness variation of microcantilevers. Meanwhile, the micromirrors require a high resolution charge-coupled device to continuously monitor the shift of reflected laser beams, and are expensive to build and use.

1.4 Need for multiple biomarkers of cancer

Despite significant progress in the investigation of cancer biomarkers, some people are over diagnosed with indolent cancer while others die from aggressive diseases that are diagnosed too late. Although several markers have reasonable operating characteristics, no individual marker is ideal. Because cancer is a polygenic disease, it is possible that a combination of biomarkers may provide better predictive value. Future research is warranted for the identification of new biomarkers, as well as novel informatics approaches to a combination of multiple biomarkers to maximize the information from currently available data.

CHAPTER 2: THERMAL DETECTION OF MULTIPLE DNA BIOMARKERS CONTAINED IN COMPLEX FLUIDS USING PHASE CHANGE NANOPARTICLES

2.1 Introduction

Current *in vitro* cancer detections and diagnosis are strongly dependent on biopsies, where tissue samples are removed from patients for analysis. Although effective in preparing samples, such invasive methods are not suitable for monitoring cancer development and treatment effects. Some cancer cells can exfoliate from the original tumors and enter the circulations, and provide an alternative way for the non-invasive or less-invasive detection and diagnosis. It is challenging, however, to detect circulating tumor cells because of their extremely low concentration (1-10 cancer cells in 1 ml blood).[50-52] As a result of fragmentation of the chromatin from dying tumor cells, tumor cells can release molecular biomarkers (i.e., DNAs and proteins) into the circulation. The circulating DNAs reflect the molecular level changes of tumors such as methylation, microsatellite instability and point mutation, and can be used for highly sensitive and less-invasive cancer detections.[53-55] In addition to less invasiveness, detecting molecular biomarkers in body fluid or cell lysate offers many benefits such as minimal sample preparation, more retention of target molecules, low cost, and short analysis time.[56-62]

Although polymerase chain reaction (PCR) and enzyme-linked immunosorbent assay (ELISA) have shown extremely high sensitivities for biomarker detection, these techniques cannot always be used to complex fluids such as cell lysate.[63, 64] The application of such

21

techniques is limited in the point-of-care due to sample preparation, equipment maintenance, and needs for skilled personnel.[65] A variety of nanoparticles with unique optical, electric, magnetic or electrochemical property have been used for *in vitro* detections of biomarkers.[66-72] By converting biological recognition events into physical signals that can be amplified, nanoparticle based methods achieve high sensitivity at the pico-mole/liter level owing to intimate contact with biomarkers in solution. However, these methods (except magnetic nanoparticle) require extensive sample preparation effort prior to detection. Otherwise, errors associated with sample preparation could be large, which will compromise their high sensitivities. For example, colored species in body fluid (i.e., red blood cell) have to be removed for optical detection; pH or salt concentration may affect the electric or electrochemical signals of nanoparticles; although magnetic signals are immune to impurities contained in samples, the signals cannot be amplified readily, and the detection sensitivity is not as high as others.[73-75]

The multistage growth of cancers is characterized by gradual accumulations of molecular genetic abnormalities associated with a range of dynamic processes such as cell cycles, senescence, apoptosis, cellular repair, differentiation and migration.[76] The diversity of cancers, combined with the complexity of each biological system, makes it difficult to detect molecular biomarker in biofluids.[77] At the early stages, biomarkers are at low concentrations and cannot be detected readily. The medical decision based on single biomarker has a high probability of false positive and false negative.[78] Thus, single biomarkers alone are not effective for accurate diagnosis. One effective way to enhance the accuracy of diagnosis is to detect multiple biomarkers from the same sample.[79] In one example, 3 to 5 biomarkers can provide more than 0.94 accuracy compared with single biomarkers.[80] Since the amount of sample obtained from a

patient is limited, and the quantity of biomarkers is very low, it is desirable to detect multiple cancer biomarkers from one sample using a highly sensitive and multiplexed method.

We have developed a method to detect short single stranded oligonucleotides (ssDNAs) in bodily fluids using solid-liquid phase changes of nanoparticles (Figure 2.1). The signal transduction is based on the thermal properties of nanoparticles by utilizing a well-known, but unexplored phenomenon, namely, the temperature of a bulk solid will not rise above its melting temperature until the solid becomes liquid completely. In the thermal test, the nanoparticle probes will melt at a narrow temperature range. The position of sharp melting peak and related heat flow are dependent on the nature of the phase change nanoparticles, and the amount of biomarkers in solution, and thus can be used for the qualitative and quantitative biomarker detection. A combination of nanoparticles with different melting temperatures can be used to detect multiple biomarkers with a high level of multiplicity. Since the melting points of nanoparticles can be designed above the melting temperatures of species contained in bodily fluids, the thermal nanoparticles can be used to directly detect molecular biomarkers in bodily fluids. The detection signals are readout using a power compensation differential scanning calorimetry, in which the heat flow added into a sample to keep its temperature the same as a reference is plotted as function of temperature. The thermal signal transduction mechanism has no macroscopic analog, but brings high sensitivity and multiplicity, as well as sample preparation benefits to the area of biomarker detections. Compared to normal micro-calorimetry of biological interactions, this approach has higher sensitivity, multiplicity, and specificity owing to the existence of thermal nanoparticles.
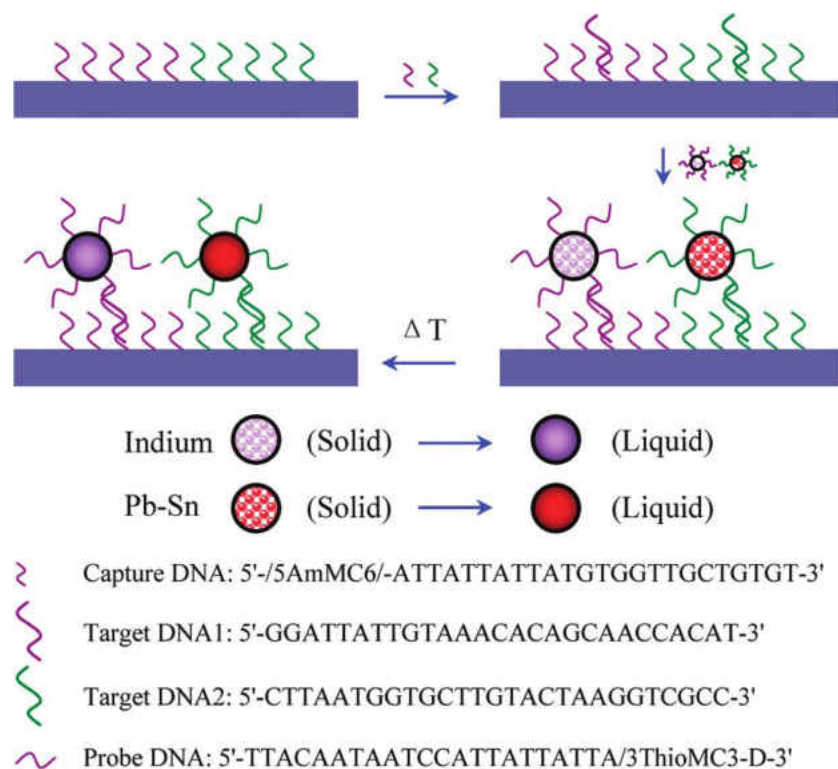
Figure 2.1 Detecting multiple DNA biomarkers using phase change nanoparticles.

2.2 Experimental and methods

2.2.1 Synthesis of nanoparticles

The phase change nanoparticles of low melting temperature metals and alloys are prepared by the thermal decompositions of organometallic precursors. The precursors, such as indium acetate, lead acetate and tin acetate are obtained from Aldrich and used without purification. The precursors or their mixtures at desired molar ratio, and polyvinylpyrrolidone (with molecular weight of 11000) are dissolved in ethylene glycol (Aldrich). The mixture is refluxed at 200°C to decompose precursors under nitrogen protection. After reacting for 20 minutes, the reaction is quenched by pouring the mixture in 200 ml ethanol pre-cooled at 0°C.

24

The as-prepared nanoparticles are centrifuged at 3000 rpm to remove un-reacted precursors, and washed by absolute ethanol for three times. A Zeiss Ultra 55 scanning electron microscope (SEM) at accelerating voltage of 10 kV is used to image nanoparticles dispersed from suspension onto a conductive silicon surface. The compositions of nanoparticles are analyzed by an energy dispersive X-ray (EDX) detector. A JEOL 1011 transmission electron microscope (TEM) operated at 100 kV is used to image the nanoparticles.

2.2.2 Surface modifications

The synthetic short oligonucleotides are obtained from Integrated DNA Technologies (IDT). The probe ssDNA is 5'-TTACAATAATCCATTATTATTA/3ThioMC3-D-3'; the target ssDNA is 5'-GGATTATTGTAAACACAGCAACCACAT-3'; and the capture ssDNA is 5'-/5AmMC6/-ATTATTATTATGTGGTTGCTGTGT-3'. The sequences of oligonucleotides are designed to be non-specific for proof-of-principle, and are not representative of any biomarkers. Figure 2.2 shows the procedure of modifying the surfaces of phase change nanoparticles, and DNA hybridization. The nanoparticles are modified with amine-terminated monolayers by adding 3-aminopropyltriethoxy-silane (APTES) into the suspension of nanoparticles in toluene. After reacting for 3 hrs at the room temperature, extra silane is removed by centrifugation, and nanoparticles are re-suspended in dimethyl sulfoxide (DMSO) that contains N-succinimidyl (4-iodoacetyl) aminobenzoate (SIAB) and incubated for 20 min to complete the reaction. The disulfide-containing probe ssDNA is reduced to 3' thiolated probe ssDNA by incubating with tris (2-carboxyethyl) phosphine (TCEP) at pH 4.5 in tris (hydroxymethyl)-aminomethane (TE) buffer at 37°C for 3 hrs. After removing excess SIAB by centrifugation, the nanoparticles are incubated with the 3' thiolated probe ssDNA in a phosphate buffer solution (PBS, pH 8.0) at the

room temperature. The aluminum surface is modified by APTES in vapor phase, where the surface is kept in a vial that contains 0.1 ml of APTES and heated for 3 hrs at 100ºC. After washing the surface with DMSO, the aluminum surface is immersed into a DMSO solution of disuccinimidyl suberate (DSS) for 1 hr. The surface is washed with PBS and incubated with capture ssDNA in PBS solution (pH 8.0) for 3 hrs. The hybridization of target ssDNA with capture ssDNA is carried out by immersing the modified aluminum surface in a target ssDNA solution of TE buffer (pH 7.5, 1M NaCl). After reacting for 3 hrs at 37ºC, unbounded capture ssDNAs are removed by washing with PBS.
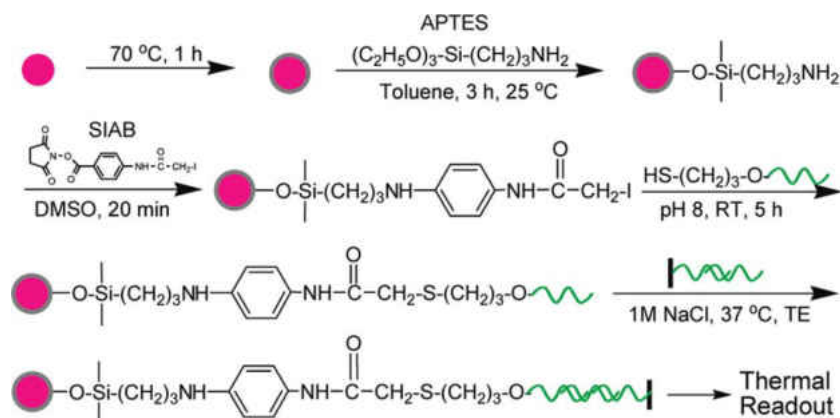
Figure 2.2 Detailed procedures of surface modification and DNA hybridization.

2.2.3 Cell lysate preparation

The MDA-MB-231 human breast cancer cells obtained from American Type Culture Collection (ATCC, Manassas, VA) are used. The cells are grown to confluence in T-75 tissue culture flasks using a protocol suggested by ATCC.   Then the culture medium is removed and the cells are washed with the PBS at pH 7.5. The cells are lysed in a 3 ml flask with lysis buffer for 15 min at 4°C with gentle rocking, where the lysis buffer is composed of 10 mM Tris-HCl at

pH 7.5, 100 mM NaCl, 1 mM EDTA, and 1% Triton X-100. The cell lysate is collected and centrifuged at 12,000 rpm for 10 min at 4°C to remove debris. The supernatant of the cell lysate is collected and stored in small aliquots at -20°C until use. The total protein concentration of cell lysate is determined to be 1.1 mg/ml using the DC Protein Assay reagent (Bio-Rad Laboratories, Hercules, CA). Bovine serum albumin is used as the standard.

2.2.4 DSC measurements

A PerkinElmer DSC (DSC 7) is used to measure the melting temperatures and fusion enthalpies of nanoparticles. For nanoparticle characterization, ~10 mg of nanoparticles is sealed inside an aluminum pan and the DSC test is carried out from 50 to 250°C at a ramp rate of 10°C per minute. An empty aluminum pan is used as reference to measure the difference in the heat flows of sample and reference. Both aluminum pans are washed for several times by ethanol and acetone. The detection sensitivity of the equipment is calibrated by measuring the fusion enthalpy of a known amount of bulk material (i.e., indium). For DNA detections, we have modified the aluminum surface with a monolayer of amine terminated molecules by APTES, because the aluminum surface is covered with a thin layer of native oxide after exposing to ambient atmosphere. The patterned immobilizations of fluorescence labeled bovine serum albumin (BSA) on the amine monolayer through covalent bonds confirm the modifications of aluminum surfaces by APTES. In order to capture the target ssDNA from samples, DSS is used to the immobilize capture ssDNA on the amine terminated aluminum surfaces.

2.3 Results and discussion

2.3.1 Phase change nanoparticles

The structures, morphologies, and thermophysical properties of indium, and lead-tin alloy nanoparticles have been confirmed by the normal characterization methods. Figure 2.3A and 2.3B show the TEM images of indium and lead-tin nanoparticles, respectively. The DSC curves confirm the solid-liquid phase changes of indium and lead-tin nanoparticles (Figure 2.3C and 2.3D), which shows the melting temperatures of indium and lead-tin nanoparticles are 156 and 183°C, respectively. Although it has been found that nanoparticles with diameter smaller than the critical diameter (~40 nm) melt at lower temperatures,[81, 82] the nanoparticles prepared here have similar melting points as bulk materials due to their large diameters. In order to modify the surfaces, the nanoparticles of indium and lead-tin alloy are dried and baked at 100°C in an oven for 1 hr. This procedure will oxidize the surfaces of low melting nanoparticles. These nanoparticles are immersed into 5% APTES in toluene for 3 hrs. After removing extra APTES by centrifuging, nanoparticles are washed by toluene and DMSO.
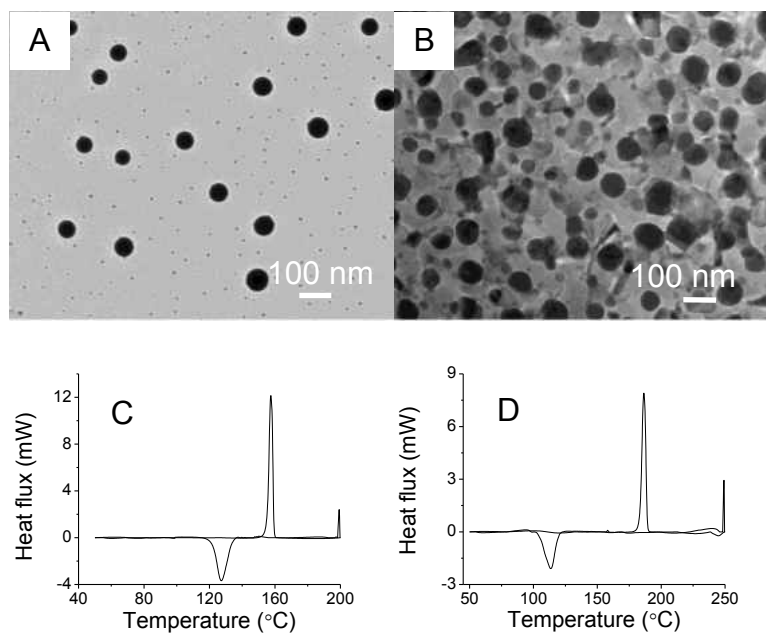
Figure 2.3 TEM images of indium (A) and lead-tin alloy nanoparticles (B); DSC curves of indium (C) and lead-tin alloy nanoparticles (D).

2.3.2 DNA detections in buffers

Target ssDNAs dissolved in phosphate buffers at pH 8.0 are studied as standard samples for DNA detection. The probe ssDNA modified nanoparticles, and capture ssDNA modified aluminum surface are added into the buffer solution for hybridization. After hybridizing for 3 hrs, the aluminum surface is taken out of the buffer solution, washed by phosphate buffer and tested by DSC. The standard samples contain a variety of concentrations of target ssDNAs from 8 nM to 0.8 fM in 1M NaCl and TE buffer. The melting peaks of phase change nanoparticles immobilized through DNA double helix are used for the qualitative and quantitative detections. Figure 2.4A shows the melting peaks of lead-tin alloy nanoparticles, where the curves from the top to bottom correspond to the concentrations of target ssDNA from 8 nM to 0.8 fM. The areas

29

of melting peaks can be derived by integrating heat flow over the melting range, and are proportional to the masses of nanoparticles or the mole numbers of target ssDNA. Figure 2.4B shows the relation between the melting peak area and the target ssDNA concentration, where a linear relation exists between the target ssDNA concentration and the peak area, and the lowest detectable concentration is determined to be 0.8 fM.
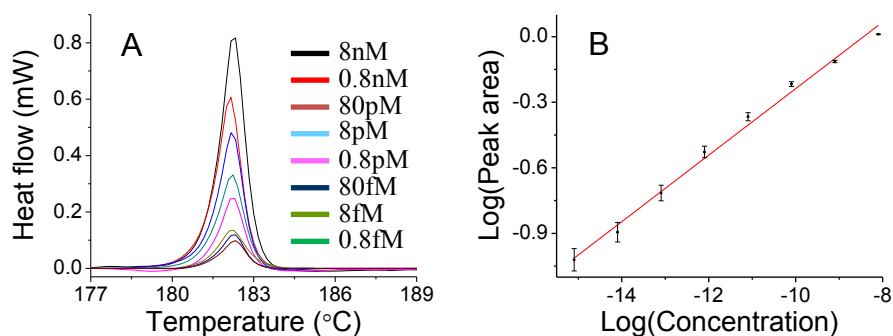
Figure 2.4 DSC curves of lead-tin alloy nanoparticles captured by target ssDNA at different concentrations in buffer solutions (A); the relation between target ssDNA concentrations and heat flows of lead-tin nanoparticles (B).

In order to test the possibility of different type of phase change nanoparticles, similarly, another type of phase change nanoparticles, indium nanoparticles, are used to detect target ssDNAs in buffers. The experiment results show that it can also be used for the detection of ssDNA in buffers. Figure 2.5A shows the DSC curves of indium nanoparticles collected at different target ssDNA concentrations. Figure 2.5B shows the relation between the measured peak area and the concentration of ssDNAs, where a linear relation exists between the target ssDNA concentration and the peak area, and the lowest detectable concentration is determined to be 80 pM.
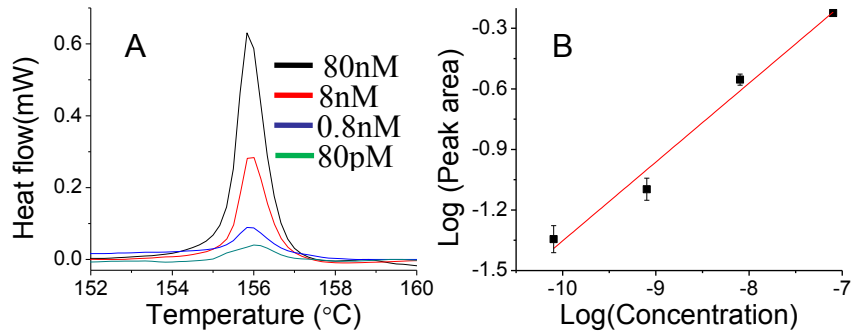
Figure 2.5 DSC curves of indium nanoparticles captured by target ssDNA at different concentrations in buffer solutions (A); the relation between target ssDNA concentrations and melting peak areas of indium nanoparticles (B).

2.3.3 DNA detections in complex fluids

Cell lysate and milk are two biological samples that contain abundant proteins and DNAs. The melting temperature of the phase change nanoparticles made in this experiment is higher than the coexisting species in cell lysate or milk, thus the thermal readout will not be interfered by species in body fluids. But, the DNA hybridization can be affected by abundant proteins or DNAs. Target ssDNAs are added to cell lysate or milk at certain concentrations, and detected using the same method described above. The pH values and ion concentrations of cell lysate are adjusted to be 10 mM Tris-HCl at pH 7.5, 100 mM NaCl, and 1 mM EDTA. Figure 2.6A shows the melting peaks of indium nanoparticles after detecting the target ssDNAs in cell lysate, where the curve from the top to bottom are collected at the concentrations of target ssDNA ranging from 8 nM to 80 pM. Although the temperature range is from 50 to 200ºC, the most parts of curves do not show any heat absorbing behaviors, thus only the thermal behavior in the range from 144 to 168ºC is displayed. Figure 2.6B shows the relation between the peak area

and the concentration of target ssDNA, from which the lowest detectable concentration is determined to be 80 pM. There exists a linear relation between target ssDNA concentrations and heat flows at relatively higher concentrations.
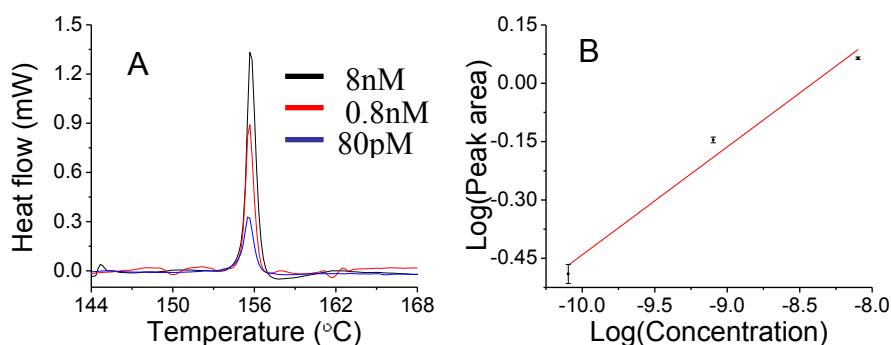
Figure 2.6 DSC curves of indium nanoparticles captured by target ssDNA at different concentrations in cell lysate (A); the relation between the target ssDNA concentrationand peak areas of indium nanoparticles (B).

Furthermore, the target ssDNA can also be detected in milk. The target ssDNA is added in fresh milk to make samples that are not transparent and detected by the same method. The pH values and ion concentrations of milk are adjusted to10 mM Tris-HCl at pH 7.5, 100 mM NaCl, and 1 mM EDTA. Figure 2.7A shows the DSC curves of lead-tin nanoparticles that are collected at different concentrations of target ssDNAs, where the melting peaks are attributed to immobilized lead-tin nanoparticles. Figure 2.7B shows the relation between the measured peak area and the concentration of target ssDNA after detecting target ssDNAs from milk.
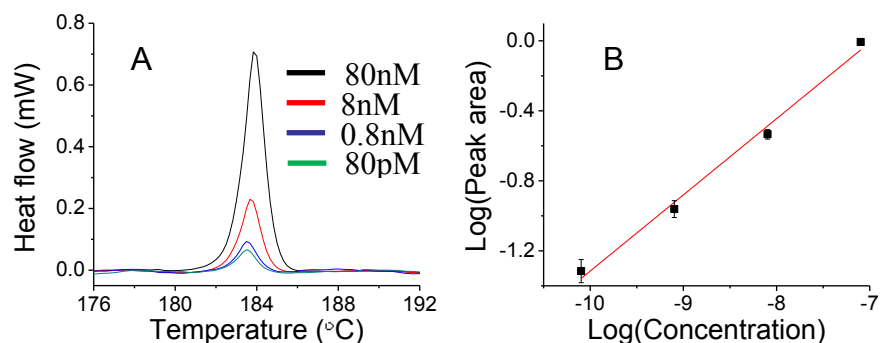
Figure 2.7 DSC curves of lead-tin nanoparticles captured by target ssDNA at different concentration in milk (A); the relations between the target ssDNA concentration and peak areas of lead-tin nanoparticles (B).

2.3.4 Comparison of DNA detections in buffers and complex fluids

Compared to buffer solutions with clearly defined composition, cell lysate and milk contain abundant proteins; meanwhile, cell lysate could also contain un-removed double-stranded DNA due to disintegration of the nuclear membrane. The proteins or DNAs can affect the detections of the target ssDNAs through either specific interaction or non-specific adsorption. We have compared the peak areas measured at different concentrations of the target ssDNAs in buffer, cell lysate, and milk. The similar level in response of heat flow means that target ssDNA has been detected. However, there are some differences in the magnitudes of peak areas: peak areas derived from the buffer solutions is similar to those from milk, suggesting that the abundant proteins (1.1 mg/ml) do not affect the hybridization of the target ssDNA very much. Instead, the heat flows measured from the cell lysate are about 20% higher than that from buffer and milk. In the cell lysis process, we have used Triton X-100 as the detergent agent to break cell membrane, which might also break the nucleus membrane and release some DNAs

into the cell lysate. It is possible some of the released DNA with sticky ends may interact with the capture ssDNA and probe ssDNA, causing the increased heat flows.

2.3.5 Detecting multiple DNA biomarkers

The sharp and discrete melting peaks of nanoparticles allow the establishment of a one-to-one correspondence between the melting peaks of nanoparticles and biomarkers, thus the method has high multiplicity. We have used this method to detect two different target ssDNAs simultaneously by modifying capture and probe ssDNAs on aluminum surfaces and two types of nanoparticles (i.e., indium and lead-tin alloy). The sequence of the first target ssDNA (ssDNA1) used to modify indium nanoparticles is the same as described above, and the sequence of the second ssDNA (ssDNA2) to modify lead-tin nanoparticles is 5'-CTTAATGGTGCTTGTACTAAGGTCGCC-3'. The capture and probe ssDNAs for the second target have the complementary sequences to each end of the second target. We have mixed the two capture ssDNAs at 1:1 molar ratio and immobilized them on one aluminum pan. Meanwhile, two target ssDNAs are dispersed in PBS at pH of 7.5 and 1M NaCl. The probe ssDNA modified indium and lead-tin nanoparticles, and the capture ssDNA modified aluminum surfaces are immersed into the PBS that contains two types of target ssDNAs for 3 hrs. After DNA hybridization, the aluminum surface is washed with a phosphate buffer and tested by DSC. Figure 2.8A shows the melting peaks of indium, and alloy nanoparticles covalently bonded on aluminum surfaces, thus confirming the existence of two types of target ssDNA in the solution.

2.3.6 Nanoparticle dependent sensitivity

The detection sensitivity is dependent on the mass and the latent heat of fusion of nanoparticles, as well as the lowest detectable heat flow of DSC. The heat energy (Q) can be derived from the mass (m) and the heat of fusion (ΔH_{fus}) of phase change nanoparticles using the following equation:

$$Q = m \cdot \Delta H_{fus} \tag{1}$$

For indium nanoparticles, the latent heat of fusion is 28.5kJ/kg. In the case of lead-tin alloy nanoparticles, the latent heat is derived to be 45kJ/kg using $H = xH_a + (1-x)H_b$, where H_a and H_b are the latent heats of two metals, and x is the mass ratio of metal A in the alloy. The minimal detectable heat flow in DSC is determined by its root-mean-square noise (0.2 μW), which corresponds an energy flow of 0.2 μJ for 1°C wide melting peak at ramp rate of 1°C/s. Assuming that nanoparticles have uniform diameters (D), and the grafting density of DNA on nanoparticle is α, the minimal number of the target ssDNA (n) that can be detected will be derived from:

$$n = \frac{3Q\alpha}{4\pi r^3 \rho \Delta H_{fus}} \tag{2}$$

where r is the radius of nanoparticle and ρ is the density of nanoparticles. From the equation, nanoparticles with large diameter or large latent heat correspond to high sensitivity. Figure 2.8B shows the relation between peak areas and target ssDNA concentrations for indium and lead-tin nanoparticles. The peak areas corresponding to indium are larger than those of lead-tin nanoparticles, which could be induced by the size difference and grafting density difference of two types of nanoparticles. Equation 2 also shows that lower grafting density corresponds to less

target ssDNA, or higher detection sensitivity. In our previous experiment on silica encapsulated indium nanoparticles, the lowest detection limit is ~8 nM because the grafting density of DNA on silica layer is higher. As a comparison, the slightly oxidized nanoparticles have lower grafting density of probe ssDNA, thus higher detection sensitivity. Providing there is only one probe ssDNA immobilized on each nanoparticle in a 1 ml solution, the accordant concentration of target ssDNA is 3.04×10^{-15} moles or 3.04 fM using indium nanoparticles under the following conditions: r is 50 nm, Q is 0.2 μJ, and ρ is 7310 kg/m^3, respectively.
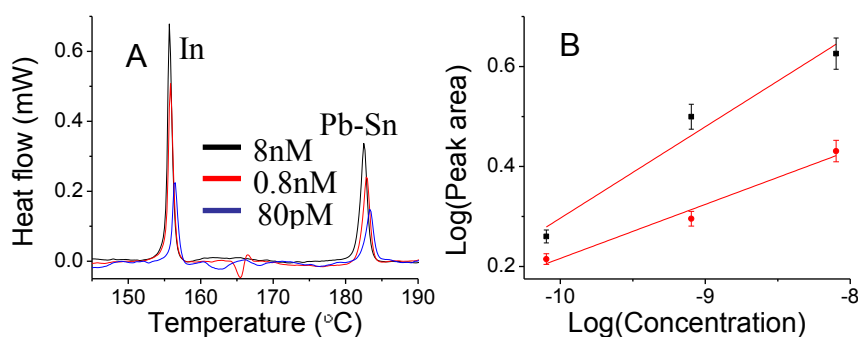
Figure 2.8 Detecting target ssDNAs in cell lysate using indium and lead-tin nanoparticles as probes (A), the relations between peak areas and target ssDNAs concentrations for indium (square) and lead-tin (circle) nanoparticles (B).

2.3.7 Multiplicity and peak width

The multiplicity of this detection method depends on the widths of melting peaks and the number of different types of nanoparticles. Not only the nanoparticles of pure metals can be used, binary or ternary alloys can be designed based on phase diagrams and produced to offer multiple types of nanoparticles. We have prepared binary alloy nanoparticles, lead-tin, that have controlled melting temperatures. The peak width is determined by two time constants: τ_i is

instrument time constant that depends on ramp rate, measuring head, atmosphere, and crucibles; τ_s is sample time constant that is a function of sample mass. Larger sample mass corresponds to larger τ_s. Considering a solid nanoparticle at its phase change temperature (T_m), the melting time depends on the size of nanoparticle and the temperature difference between the surface temperature of nanoparticle and the melting temperature of nanoparticle material:

$$\frac{(T_s - T_m) \cdot \tau}{\left(\dfrac{\rho_l Q_l}{k_l}\right)} = r_p^2 \left[\frac{1}{3}\left(\frac{r}{r_p}\right)^3 - \frac{1}{2}\left(\frac{r}{r_p}\right)^2 + \frac{1}{6} \right] \tag{3}$$

where T_s and T_m are the surface temperature and the melting point of nanoparticles, respectively; τ is the melting time when the solid radius is r, r_p is the radius of the nanoparticle before melting; Q_l is the latent heat of fusion of nanoparticles; k_l is the thermal conductivity of nanoparticles; and ρ_l is the density of nanoparticles. For the indium nanoparticles, k_{In} is 81.8 W·m^{-1}·K^{-1}, r_{In} is 50 nm, Q_{In} is 28.52 kJ/kg, and ρ_{In} is 7310 kg/m^3, respectively. Replacing all the symbols with numbers, we can derive that τ is 0.11 µs. Figure 2.9A shows the simulated melting time of a 100 nm indium nanoparticle as functions of the difference between the surface temperature and the melting temperature of nanoparticles. From the curves, the melting time is less than 100 µs at the ramp rate of 10ºC per minute, and the temperature difference of 0.1ºC. The contribution of nanoparticle melting on peak width is smaller than those taken by instrument. Figure 2.9B shows ramp rate dependent full width at half maximum (FWHM) of melting peaks measured for indium and alloy nanoparticles. In both cases, the peak width becomes smaller as the ramp rate is decreased. A linear relation exists between ramp rate and peak width, and the smallest peak width among all ramp rates studied is 0.3°C. Therefore, providing a sufficient number of

different alloy nanoparticles can be made with controlled melting temperatures, the multiplicity

of this method can be as high as 1,000 for the temperature scan range of 100 to 700ºC.
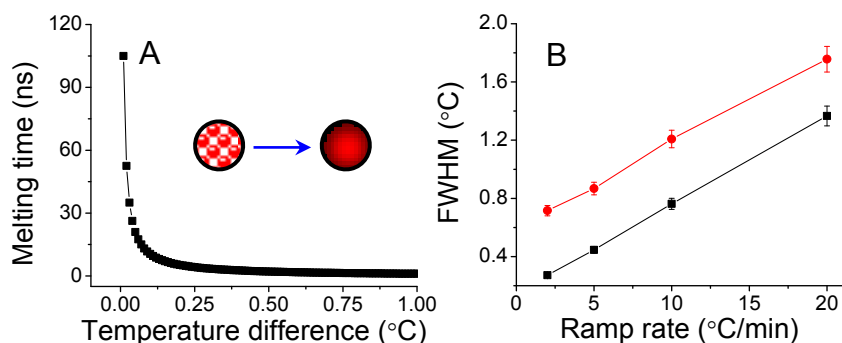
Figure 2.9 The melting times of indium nanoparticles with diameter of 100 nm as the function of the temperature difference between surface and melting temperature (A); the ramp rate dependent peak width for indium (square) and lead-tin alloy (circle) nanoparticles (B).

2.4 Conclusions

We have shown the capability of thermally addressed nanoparticles for the detection of

molecular biomarkers by using phase change nanoparticles of metallic materials (i.e., pure metal

and alloy). The novel signal transduction mechanism allows the detections of multiple DNA

biomarkers in cell lysate and milk with high sensitivity, which is comparable to other

nanoparticle based methods. In addition, the melting peaks and fusion enthalpies measured from

the temperature scan processes can be used for the qualitative and quantitative detections of

biomarkers.

CHAPTER 3: MULTIPLEXED PROTEINS DETECTION USING PHASE CHANGE NANOPARTICLES

3.1 Introduction

Detecting protein biomarkers in complex fluids such as blood, urea, or cell lysate offers great benefits in sample preparation and target retention for early disease detection.[83-85] Enzyme-linked immunosorbent assay (ELISA) relies on antigen-antibody interaction to detect antibodies (i.e., proteins), and the binding events are readout through enzyme activities or the physical, chemical, or spectroscopic labels attached on the antibodies at different sites.[86-88] Because of the small sizes, nanoparticles have intimate contacts with target proteins in solutions and have been used to detect specific antigen-antibody interaction,[89-92] where the sensitivity is enhanced by amplifying the physical signatures of nanoparticles. Although widely used, ELISA has some limits: (1) it requires extensive efforts and expensive agents to produce testing samples that are free of colored species, suitable pH, and salt concentration; species that interfere with the activity of enzyme should be removed; (2) the multiplicity is often low, even if nanoparticles are used as probes, which makes it hard to detect multiple proteins from a small amount of sample. In this aspect, although optical absorbances of metallic and semiconductor nanoparticles can be controlled in the range of 400-900 nm by changing diameters,[93] the absorbance or emission peaks in this region are wide (~150 nm), which limits the number of biomarkers that can be detected in one assay due to peak overlap.[94] Metal or magnetic nanoparticles cannot be used to detect multiple proteins because different nanoparticles are not distinguishable by their electric

or magnetic properties.[95-98] The electrochemical method can detect a few types of nanoparticles but the peaks are wide and the voltage range is narrow (few voltages), which limits its detection multiplicity.[99]

We describe a novel technique that depends on the solid-liquid phase transitions of nanoparticles to detect multiple proteins. In this thermally addressed immunosorbent assay (TAISA), pure metal or alloy nanoparticles with a variety of compositions and melting temperatures are made by the colloidal method and modified by antibodies. A solid surface (i.e., aluminum) is also modified by antibodies;[100] the aluminum surface is immersed in a solution that contains the target antigen. After washing, the aluminum surface is immersed in a solution containing nanoparticle-labeled antibody (Figure 3.1). In this sandwich detection configuration, the thermal property of the immobilized nanoparticles is directly measured rather than that of the antigen-antibody interaction. The signal transduction is based on a known but unexplored phenomenon: the temperature of a single component solid does not rise over its melting point until the entire solid is molten,[101] thus the melting peak of the solid is sharp after a linear temperature rise process. A one-to-one correspondence can be created between the melting point of one type of nanoparticles and one type of protein. The melting temperature and the heat flow are used to distinguish and quantify the nature and concentration of the protein. Because the melting temperature of the nanoparticles can be designed to be higher than those of the species contained in samples, the method is immune to colored or conductive species. In addition, the method can detect multiple proteins due to sharp melting peaks and multiple choices of phase change materials (i.e., metal, alloy, polymer, and salt). In a typical thermal scan from 20 to 700 °C, the number of different types of nanoparticles that can be detected in one run will reach 1000

40

if the peak width at half-maximum is 0.6 °C, meaning that the method has a high level of multiplicity.
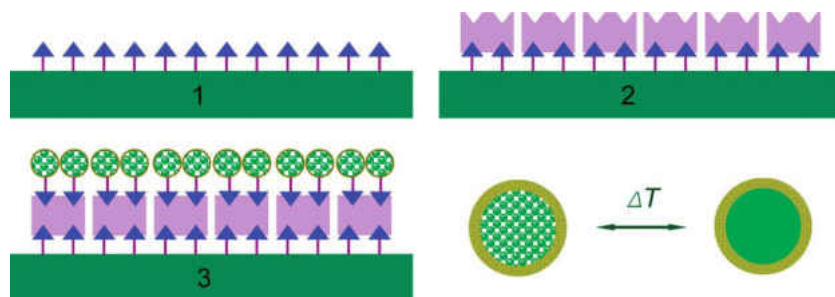
Figure 3.1 Schematic illustration of thermally-addressed immunosorbent assay.

3.2 Experimental and methods

3.2.1 Synthesis of phase change nanoparticles

All chemicals used in this experiment are obtained from Sigma-Aldrich. The phase change nanoparticles of pure metals and alloys such as indium, tin, and lead-tin alloy nanoparticles are prepared by thermal decompositions of organometallic precursors.[102-104] The precursors are dissolved, or two types of precursors are mixed at a stoichiometric ratio and dissolved into ethylene glycol (EG) in the presence of polyvinyl-pyrrolidone (PVP). These precursors are decomposed at 200 °C under protection of nitrogen. After reacting for 30 min, the reactions are quenched by pouring the liquid into 200 mL of ethanol that is precooled at 0 °C. Then the nanoparticles are separated by using centrifugation, washed by ethanol three times, and dried with nitrogen flow for future use.

3.2.2 Nanoparticle characterizations

A ZeissUltra 55 scanning electron microscope (SEM) working at an accelerating voltage of 10 kV is used to image nanoparticles that are dispersed from suspension onto a conductive silicon surface. The compositions of nanoparticles are confirmed by an energy dispersive X-ray (EDX) detector. A JEOL 1011 transmission electron microscope (TEM) that is operated at 100 kV is used to image the nanoparticles. The melting temperatures and the fusion enthalpies of nanoparticles are measured by using a differential scanning calorimeter (PerkinElmer DSC 7). A total of 5 mg of nanoparticles is sealed inside an aluminum pan and tested from 50 to 300 °C at a temperature ramp rate of 10 °C/min. An empty aluminum pan is used as reference to determine the difference in heat flow of the sample and the reference. The differential scanning calorimetry (DSC) experiments provide heat fluxes in both melting and crystallization processes, but only melting curves are used in this work. The enthalpies of fusion of the nanoparticles are derived from peak areas using the data analysis software of the DSC instrument. From the latent heats of fusion, the amount of phase change nanoparticles can be derived. The melting temperatures of indium, lead-tin, and tin nanoparticles are determined to be 156, 183, and 230 °C, respectively, which are the same as the bulk counterparts because of the large diameters.[105-107] Lead-tin alloy nanoparticles at the eutectic compositions have also been prepared by this method. The size and shape of indium and lead-tin alloy nanoparticles has been characterized by TEM and it has been mentioned in chapter 2 and section 2.3.1. For tin nanoparticles, Figure 3.2A shows a typical TEM image and it shows that the nanoparticles have the size of about 100 to 200nm. Figure 3.2B shows the DSC curve of tin nanoparticles, it shows that the melting temperature of tin nanoparticles is about 231°C. The crystallized structures of nanoparticles at room temperatures

have been confirmed by selected area electron diffraction (SAED). Some of the characterization results such as SEM images, SAED patterns, and DSC curves can be found in our previous papers.[108]
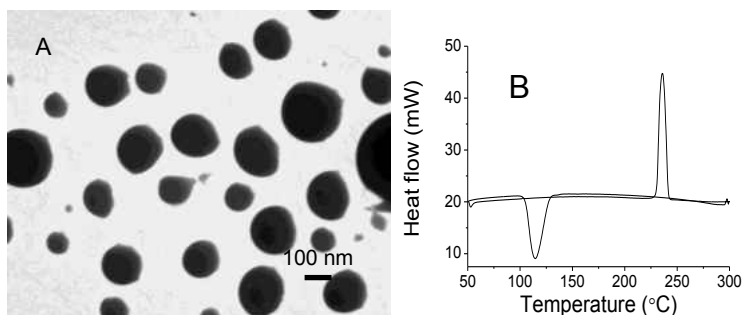
Figure 3.2 (A) TEM image of tin nanoparticles; (B) DSC curve of tin nanoparticles.

3.2.3 Surface modification of nanoparticles

The surface modifications of nanoparticles are carried out as follows. The lead-tin nanoparticles are dried and heated to 100 °C in an oven in atmosphere, which produces thin layers of oxide around nanoparticles. The existence of a thin oxide layer has been verified by using energy dispersive X-ray analysis (EDX), which has been shown in Figure 3.3A. The oxide layer of the nanoparticle is amine-modified by incubating in 10% (aminopropyl) triethoxysilane (APTES) in toluene for 1 h at room temperature, which is followed by washing in toluene and in PBS solution. The surface modification of nanoparticles is confirmed by using fluorescent labeled bovine serum albumin proteins (BSA), which are covalently immobilized onto nanoparticles using a bifunctional cross-linker, disuccinimidyl suberate (DSS). Figure 3.3B shows a fluorescent image of BSA modified lead-tin nanoparticles. Furthermore, we have shown

the surface oxidation of lead-tin thin films at the same heating conditions, where the thin film is patterned to indicate fluorescent contrast. Lead-tin thin films are deposited onto silicon surfaces using electron beam evaporation. Then thin layers of photoresist are spun onto the films and exposed with UV light through a photo mask that has patterns. After development of exposed portions, the films are treated in APTES vapor at 100 °C, which is followed by removing unexposed photoresist. In the next, fluorescent BSA proteins are immobilized onto amine-modified surfaces by using DSS as crosslink. The micropattern on the lead-tin thin film can be seen under a fluorescent microscope as shown in Figure 3.3C, confirming the oxidization and modification of the lead-tin film. Similar modifications have been done on thin films of tin and indium.
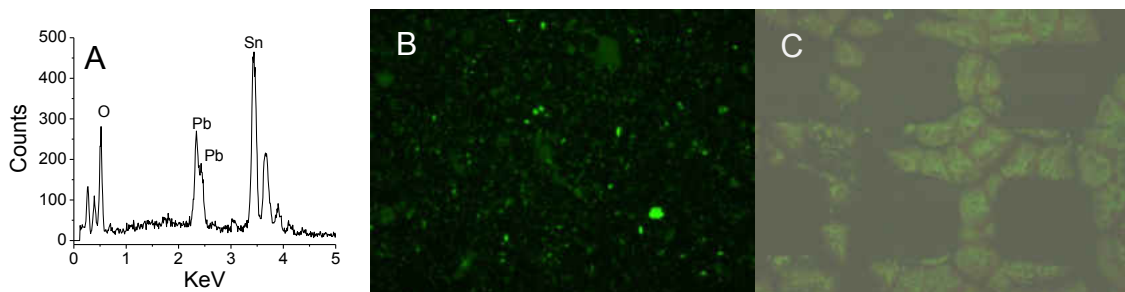
Figure 3.3 (A) EDX collected from surface-oxidized lead-tin nanoparticles; (B) a fluorescent image of BSA modified lead-tin nanoparticles; (C) a fluorescent micro-pattern on the lead-tin thin film.

3.2.4 Surface modification of aluminum surfaces

In order to immobilize ligands on surface, the native oxide film on an aluminum surface is modified by putting the surface in a small vial that contains 0.1 mL of APTES. The vial is then heated in an oven at 100 °C for 1 h. The APTES vapor will condense and react with oxide

surface to form an amine-terminated monolayer. The EDX spectrum confirms the oxidation and modification of aluminum. Figure 3.4A and 3.4B show the EDX spectra of aluminum surface before and after modification by APTES, respectively. The oxygen characteristic absorption peak in Figure 3.4A verified an aluminum oxide thin layer coated on the aluminum surface, while the silicon and nitrogen absorption peak in Figure 3.4B confirmed the successful chemical modification of the aluminum surface by APTES. The surface modification has also been further confirmed by immobilizing fluorescent BSA proteins on an aluminum surface with micropatterns. After the surface was washed with dimethyl sulfoxide (DMSO), the amine-terminated surface is immersed in an anhydrous DMSO solution containing DSS for 1 h. The surface is washed three times using DMSO and phosphate buffered saline (PBS), respectively, and then incubated with fluorescent labeled BSA protein in PBS for 2 h. The unreacted proteins are removed by washing thoroughly with PBS. Figure 3.4C shows the fluorescent micropatterns on the aluminum surface. It is clearly suggesting the successful modification of the aluminum surface after following our surface modification procedure.
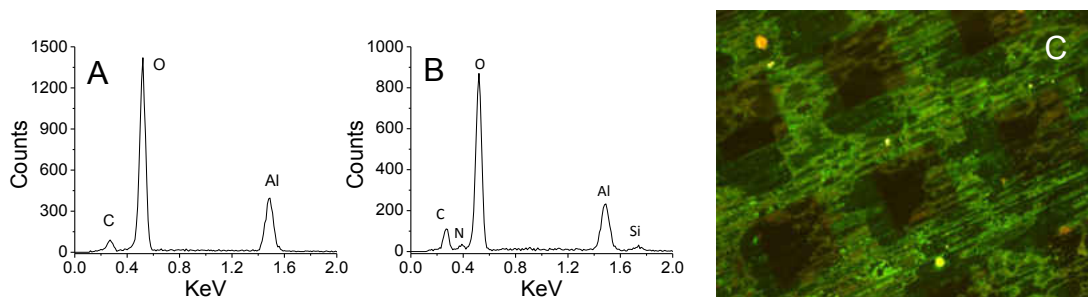
Figure 3.4 EDX spectrum collected from an aluminum surface before (A) and after (B) modified by APTES; (C) a fluorescent micro-pattern on the aluminum surface.

3.3 Results and discussion

3.3.1 Thermal detections of avidin in buffers

The thermally address method is used to detect avidin in buffer by using phase change nanoparticles of indium and lead-tin alloy. The nanoparticles are modified to have amine groups. The aluminum surface with native oxide is also modified to have amine groups. The amine-modified nanoparticles and the aluminum surfaces are conjugated with biotins by incubating with amine reactive biotinylation reagent (NHS-LC-biotins) in anhydrous DMSO for 1 h at room temperature, which is followed by washing in DMSO and in PBS. The avidin detection is carried out by incubating the biotin modified aluminum surface in solutions that contain avidin at certain concentrations for 1 h. The surface is then incubated in biotin modified nanoparticles for 1 h after rinsing. Unconjugated nanoparticles are rinsed away, and immobilized ones are readout using DSC. Figure 3.5A shows the DSC curves of indium nanoparticles immobilized on aluminum surfaces at different avidin concentrations, where the thermal scan is carried out from 50 to 300 °C at a ramp rate of 10 °C/min. The single melting peaks at 156 °C confirm that indium nanoparticles have been immobilized onto aluminum surfaces. The measured heat flows decrease as the concentrations of avidin decrease (Figure 3.5B).
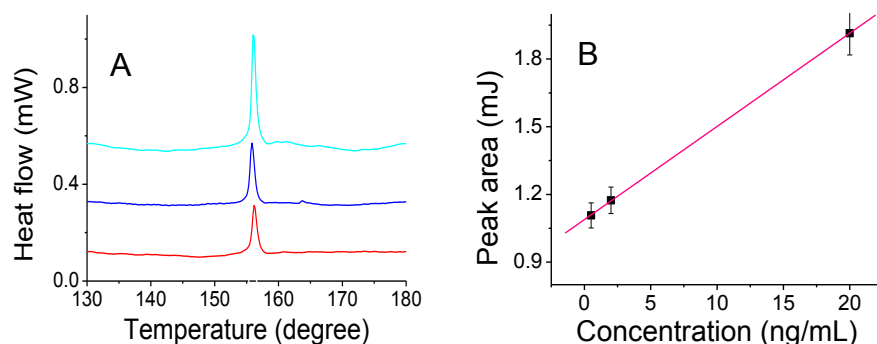
Figure 3.5 DSC curves (A) and concentration dependent heat flows (B) of indium nanoparticles that are immobilized on aluminum surfaces through biotin-avidin interaction, where the curves from up to down are at avidin concentrations of 20, 2, and 0.05 ng/mL, respectively.

Similarly, we have also used lead-tin nanoparticles (atomic ratio of 63:37) to detect avidin in buffers. The avidin detection is carried out by incubating the biotin modified aluminum surface in solutions containing different concentrations of avidin for 1 h. The surface is incubated in biotin modified lead-tin nanoparticles for 1 h after rinsing. After the aluminum surface is rinsed, the thermal signatures of lead-tin alloy nanoparticles are read out using DSC at a ramp rate of 10 °C per min. Figure 3.6A shows the DSC curves of the lead-tin alloy nanoparticles immobilized on aluminum surfaces at different avidin concentrations, where nanoparticles melt at 183 °C, and the heat flows decrease linearly as avidin concentration reduces (Figure 3.6B).

Figure 3.6 DSC curves (A) and concentration dependent heat flows (B) of lead-tin nanoparticles that are immobilized on aluminum surfaces through biotin-avidin interaction, where the curves from up to down are at avidin concentrations of 200, 20, 0.5, and 0.2 ng/ml, respectively.

3.3.2 Thermal immunoassay in buffers

The thermal immunoassay using phase change nanoparticles is carried out as follows. The amine-modified nanoparticles and the aluminum surface are conjugated to anti-rabbit IgG by incubating them with DSS in anhydrous DMSO in PBS (pH of 7.4) for 2 h. The nanoparticles and the aluminum surface are then washed by PBS to remove excess DSS. The anti-rabbit IgG modified aluminum surface is incubated in solutions containing rabbit IgG at a certain concentration for 1 h. The surface is incubated in anti-rabbit IgG modified lead-tin nanoparticles for 1 h after rinsing. After the aluminum surfaces are rinsed, the lead-tin nanoparticles are read out using DSC. Figure 3.7A shows the melting peaks of lead-tin nanoparticles immobilized at different concentrations of rabbit IgG. The crossreactivity (selectivity) has been checked by human IgG (bottom curve), where 20 ng/mL human IgG does not lead to immobilization of nanoparticles. Figure 3.7B shows that the heat flow is proportional to the concentration of rabbit IgG.
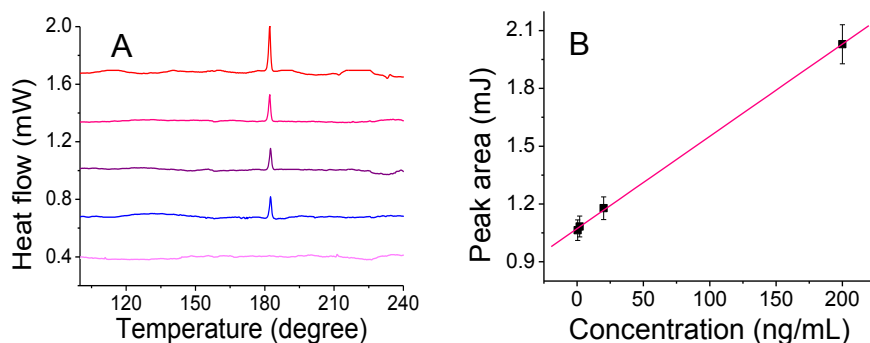
Figure 3.7 DSC curves (A) of lead-tin nanoparticles at 200, 20, 2, and 0.5 ng/ml (top to down) of rabbit IgG; 20 ng/ml of human IgG does not cause attachment of nanoparticles (flat line); the relation between the heat flow (peak area) and rabbit IgG concentration (B).

In addition, human IgG in buffer is detected using tin nanoparticles in PBS (pH of 7.4). The surfaces of tin nanoparticles and aluminum surfaces are first modified with antihuman IgG. The antihuman IgG modified aluminum surface is incubated in solutions containing human IgG at a certain concentration for 1 h. The surface is incubated in antihuman IgG modified nanoparticles for 1 h after rinsing. Figure 3.8A shows the melting peaks of tin nanoparticles immobilized on aluminum surfaces at several human IgG concentrations, where the nanoparticles melt at 230 °C and the heat flows decrease as the concentrations of human IgG reduce (Figure 3.8B). Each DSC curve is flattened by using the commercial software of the DSC instrument to remove the slope, which is induced by a heat transfer difference between the sample cell and the reference cell.
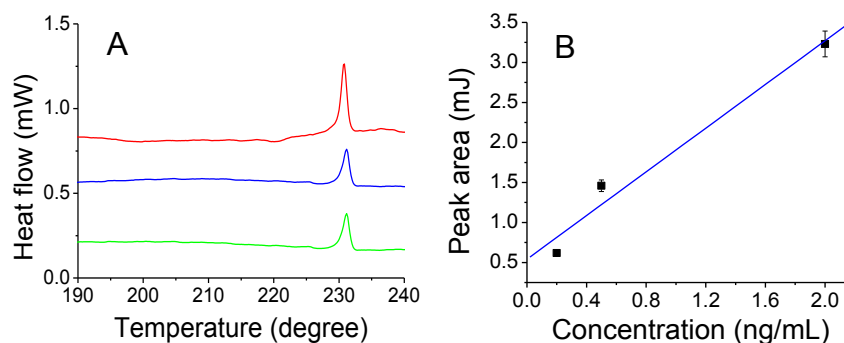
Figure 3.8 DSC curves (A) of tin nanoparticles that are immobilized at 2, 0.5, and 0.2 ng/ml (top to down) of human IgG; the relation between the heat flow and human IgG concentration (B) after immobilization of tin nanoparticles

3.2.3 Multiplexed thermal immunoassay in buffers

The multiplicity of thermal detection is reflected in the simultaneous detection of rabbit IgG and human IgG, where lead-tin nanoparticles and tin nanoparticles are modified with anti-IgGs of the rabbit and human, respectively. In order to modify aluminum surfaces, both anti-IgGs of the rabbit and human are mixed at the same molar ratio and immobilized on amine-ended aluminum surfaces. The multiplexed detection is done by incubating the modified aluminum surface in a mixture that contains 2 ng/mL rabbit IgG and 2 ng/mL human IgG in PBS (pH 7.4) for 1 h. After the surface is rinsed, it is incubated in a mixture of two types of modified nanoparticles for 1 h. The aluminum surface is tested by DSC after rinsing for a second time. Figure 3.9A shows two melting peaks of tin and lead-tin nanoparticles at 183 and 230 °C, respectively. The difference in the heat flows of the two peaks may be induced by differences in latent heats of indium and lead-tin alloy with sizes of two types of nanoparticles or grafting

densities of anti- IgGs on them. The one-to-one correspondence created between protein and melting temperature allows the detection of multiple proteins in one experiment.

The multiplicity of the thermal method is dependent on the sharpness of individual peaks due to the issue of peak overlap. Figure 3.9B shows the relation between the ramp rate and the peak width at half height of the indium nanoparticles, where the peak width is proportional to the ramp rate and the minimal peak width is 0.6 °C. Considering the composition-dependent melting temperatures of alloys, nanoparticles with different melting temperature can be designed to have a large number of melting peaks based on phase diagrams. The sharp melting peaks, combined with the large number of different melting peaks of nanoparticles, enhance the multiplicity of detection by operating DSC at a low ramp rate.
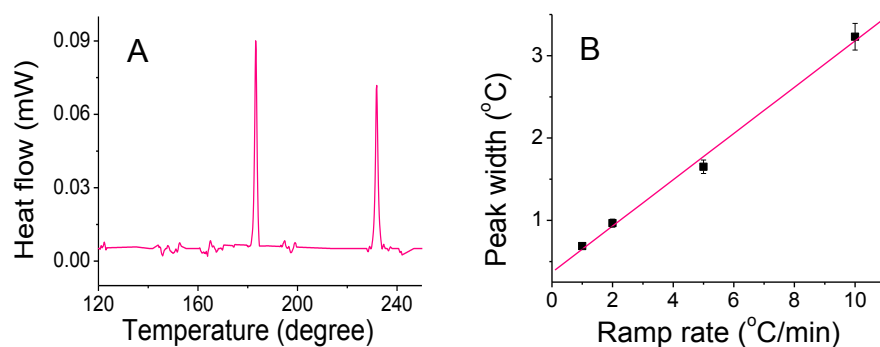
Figure 3.9 DSC curve of the multiplexed detection of 2 ng/mL of human IgG and 2 ng/mL of rabbit IgG using tin nanoparticles and lead-tin nanoparticles, respectively (A); ramp rate dependent peak width for indium nanoparticles (B).

3.2.4 Thermal immunoassay in cell lysate

The thermal immunoassay has been carried out in a complex cell lysate of human breast cancer cells. The cell lysate contains a certain amount of human IgGs released from cell membranes. At first, rabbit IgGs are added at a certain concentration in diluted cell lysates (total protein concentration is determined to be 1 μg/mL). The anti-rabbit IgG modified aluminum surfaces are incubated in solutions containing different concentration of rabbit IgG for 1 h. The surface is incubated with anti-rabbit modified nanoparticles for 1 h after rinsing. After the surface was rinsed again, the thermal signatures of the lead-tin nanoparticles are read out using DSC at a ramp rate of 10 °C/min. Figure 3.10A shows the DSC curves of lead-tin nanoparticles immobilized on aluminum surfaces at different rabbit-IgG concentrations, where the heat flows decrease as the concentration of rabbit IgG decreases (Figure 3.10B).

The concentration of human IgG in the diluted cell lysate (total protein concentration of 1 μg/mL) is determined by using antihuman IgG modified lead-tin alloy nanoparticles and aluminum surfaces. The surface modifications are carried out by using the same method as before. The antihuman IgG modified aluminum surface is incubated in the lysate for 1 h. The surface is incubated with antihuman IgG modified lead-tin nanoparticles for 1 h after rinsing. Then the aluminum surfaces are taken out, washed using PBS to remove excess nanoparticles, and analyzed using DSC at a ramp rate of 10 °C/min. Figure 3.10C shows the melting curve of lead-tin nanoparticles immobilized on the aluminum surface. From the peak area, the concentration of human IgG in the dilute lysate (1 μg/mL total protein) is determined to be 182 ng/mL. As a rough comparison, 20% of proteins contained in normal human serum are IgG.[109] If this value is valid for the human cancer cells in this study, the estimated concentration of human

IgG (with total protein concentration of 1 μg/mL) would be 200 ng/mL, which is as the same order as the value we have derived using lead-tin nanoparticles.
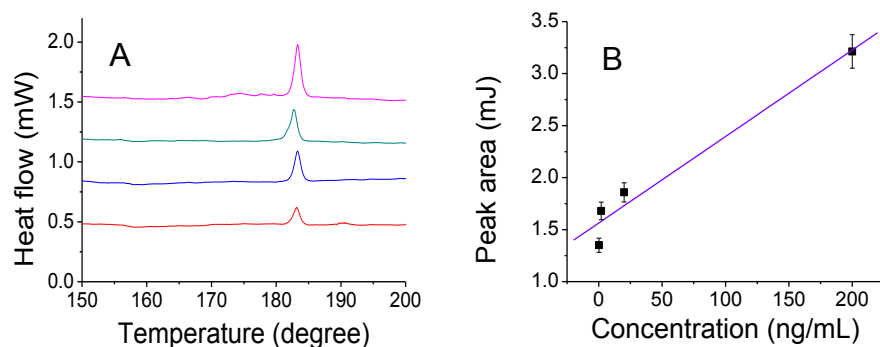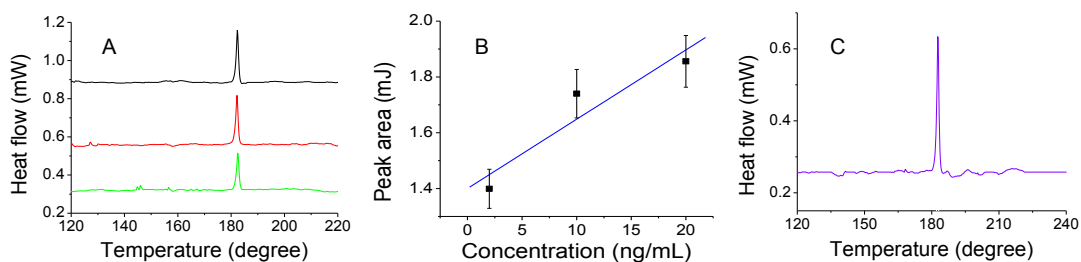

Figure 3.10 DSC curves (A) and concentration dependent heat flow (B) of lead-tin nanoparticles that are immobilized on aluminum surfaces by anti-rabbit-IgG and rabbit IgG interaction in diluted cell lysate, where rabbit IgG is intentionally added into the complex liquid at concentrations of 20, 10, and 2 ng/mL (top to bottom); DSC curve of lead-tin nanoparticles that are immobilized by human IgG contained in the diluted cell lysate (C).

3.4 Conclusions

In conclusion, we have shown the multiplexed detection of proteins using solid-liquid phase change nanoparticles as thermally addressed barcodes. A one-to-one correspondence is established between the type of nanoparticles and the type of proteins, thus multiple proteins can be detected simultaneously by using a combination of nanoparticles. The sensitivity can be further enhanced using nanoparticles with a large latent heat of fusion and reducing the grafting density of the antibody on the nanoparticle. The melting peak and heat flow reflect the nature and concentration of the protein, respectively. The melting temperature of the nanoparticles can be designed to avoid interference from coexisting species in samples, thus bringing high sensitivity and multiplicity and sample preparation benefits to the early detection of proteins. At

last, the method is generic and can be used for the detection of disease markers in various body fluids.

CHPATER 4: HIGHLY-SENSITIVE THERMAL DETECTION OF THROMBIN USING APTAMER-FUNCTIONALIZED PHASE CHANGE NANOPARTICLES

4.1 Introduction

Thrombin is one kind of physiological protease found in the blood, which can convert soluble fibrinogen into insoluble strands of fibrin, causing blood clotting. Thrombin is also involved in a number of biological processes such as cardiovascular diseases, metastasis, angiogenesis, regulation of tumor growth, and has been used as a biomarker for tumor diagnosis.[110-112] The concentration of thrombin in blood can change considerably from nM to low μM levels; in patients with coagulation abnormalities thrombin circulates at much lower concentration at pM level.[113, 114] For the cancer marker thrombin-antithrombin (TAT) complex, the concentration of thrombin in blood samples is as low as 2.0 ng/ml.[115] Developing an assay with high sensitivity, selectivity, and simplicity for thrombin detection can greatly facilitate the diagnosis and cure of related diseases.

Enzyme-linked immunosorbent assay (ELISA) has been widely used for sandwiched detections of proteins, where specific antibodies are immobilized onto a substrate to capture target proteins; another antibody is then attached onto the other side of proteins to report the binding event.[116-119] Instead of using antibodies that are delicate to handle, target proteins can also be captured by DNA and RNA aptamers, which are single-stranded nucleic acids that can bind to protein targets with high specificity. Aptamers can be selected from random libraries

using an in vitro evolution process known as SELEX or systematic evolution of ligands by exponential enrichment.[120-122] Compared to conventional antibodies, aptamers offer certain advantages in terms of high binding specificity, good stabilization, low cost, ease of preparation, storage and modification.[123-126] The signal transductions after binding of aptamers or antibodies are based on the physical, chemical or biological properties of reporting probes, and can be amplified thereafter to achieve high sensitivity. Until now, various aptamer-based sensors have been used for thrombin detection. These sensors depend on well-established signal transduction mechanisms such as optical transduction, mass spectroscopy, fluorescence, colorimetry and electrochemistry.[127-136] Microfluidic devices have also been used for aptamer-based thrombin detection.[137] Although successful from one or more aspects of detection, most of these techniques suffer from complexity, reliability, selectivity and sensitivity issues.

The advent of nanostructured materials has brought many opportunities to dramatically enhance sensitivity of bio-detections. Because of their unique electrical and optical properties, nanoparticles-based materials have provided excellent prospects for chemical and biological sensing.[138, 139] Metal nanoparticles, with controlled size, shape, and structure can be made using simple colloid-chemical methods.[140-142] The surface properties of nanoparticles can be engineered, and appropriate ligands can be conjugated through various surface modifications.[143-146] Owing to their small size and large surface area, nanoparticles can have intimate contact with target analytes in solution. After immobilizing specific ligands (i.e., aptamers or antibodies) onto nanoparticles, the specific binding can be readout through changes in the physical, chemical, or biological properties of the reporting probes. The biological recognition events are converted to physical signals that can be amplified to reflect the presence

and the amount of target molecules.[147, 148] But, existing nanoparticle based detection methods (except magnetic nanoparticle one) need extensive sample preparation efforts to remove colored or interference species prior to analysis; otherwise, errors from sample preparation will be overwhelming, resulting in the reduction of detection performance. In particular, for thrombin detection in strongly colored blood samples, thrombin can stick irreversibly onto container walls or be lost during sample handling. An ideal way for thrombin detection would be one that requires less effort for sample preparation and at the same time offer high sensitivity and high specificity.

We report a new nanoparticle-based scanning calorimetric method for thrombin detection by using aptamer-functionalized phase change nanoparticles as thermal probes. The signal transduction is based on the thermal properties of nanoparticles by utilizing a well-known, but unexplored phenomenon: namely, the temperature of a bulk solid will not rise above its melting point until all solid is molten completely. In this method, the melting enthalpy of nanoparticles is directly measured instead of that of aptamer-protein interaction. The position and area of the melting peak are used to recognize and quantify the presence and amount of thrombin, respectively. This method is immune to colored species (red blood cells) in sample, and can be performed in blood samples directly. Briefly, nanoparticles of low melting point materials are modified with thrombin aptamer; flat substrates (aluminum or filter paper) and nanostructured substrates (silicon nanopillar array) are also modified by aptamer; the aptamer modified surface is immersed into a buffer solution or fetal calf serum buffer solution that contains thrombin; the binding of aptamer modified nanoparticles with thrombin results in immobilization of the

nanoparticles in sandwiched configuration, where the nanoparticles can be readout easily using a differential scanning calorimetry (DSC) (Figure 4.1).
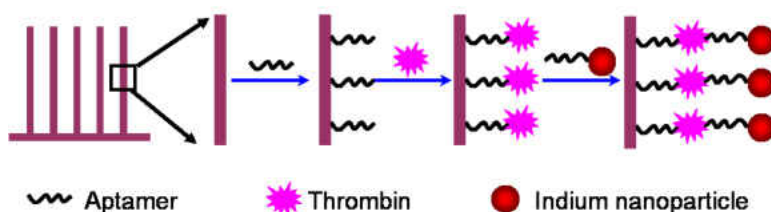
Figure 4.1 Thermal detection of thrombin using aptamer-functionalized phase change nanoparticles.

4.2 Experimental sections

4.2.1 Chemicals and materials

Human thrombin, fluorescein isothiocyanate-labeled bovine serum albumin (FITC-BSA), indium acetate, ethylene glycol, and polyvinylpyrrolidone were purchased from Sigma-Aldrich (St. Louis, MO). The thrombin aptamer with sequence of 5'-AmMC6-TTT TTT TTT TTT TTT GGT TGG TGT GGT TGG-3' was designed using systematic evaluation and obtained from IDT (Coralville, IA). The aptamer was dissolved in pH 7.4 phosphate saline (PBS) buffer (0.01 M in phosphate, 0.14 M NaCl, 2.7 mM KCl) unless otherwise noted. Anhydrous dimethyl sulfoxide (DMSO), Whatman filter paper (grade 1), toluene, 3-aminopropyltriethoxysilane (APTES), hydrogen peroxide (H_2O_2), sulfuric acid (H_2SO_4), and hydrogen fluoride (HF) were obtained from VWR (West Chester, PA). Disuccinimidyl suberate (DSS) was obtained from Thermo Scientific (Waltham, MA). Surfactant free carboxyl-modified polystyrene (PS) suspension (400 nm of diameter) containing 4% solid, and fetal calf serum were obtained from Invitrogen

(Carlsbad, CA). Ultrapure water (18.2 MΩ cm) purified by nanopure System (Barnstead, Kirkland, WA) was used throughout the experiments. All chemicals used in this study were analytical reagent grade.

4.2.2 Synthesis and characterization of phase change nanoparticles

Phase change indium nanoparticles with melting temperature of 156ºC were made by thermal decomposition of organometallic precursors (indium acetate). The precursor and polyvinylpyrrolidone (molecular weight of 11000) were dissolved in ethylene glycol and stirred for 10 minutes to make a homogeneous solution. After the mixture was refluxed at 200°C for 20 minutes to decompose precursors under nitrogen protection, the product was quenched by pouring the mixture in ethanol pre-cooled at 0°C. The as-prepared nanoparticles were centrifuged at 3000 rpm for 10 minutes. After removing supernatant, the nanoparticles were resuspended in ethanol and centrifuged again. This process was repeated three times to ensure that nanoparticles were clean. A JEOL 1011 transmission electron microscope (TEM) operated at 100 kV was used to derive the size and shape of the synthesized nanoparticles. A Zeiss Ultra 55 scanning electron microscope (SEM) at accelerating voltage of 10 kV was used to image nanoparticles. The compositions of nanoparticles were analyzed by using an energy dispersive X-ray (EDX) detector.

4.2.3 Fabrication of nanostructured Si surfaces

Silicon nanopillar arrays with high aspect ratio were created by a metal assisted etching method.[149] Briefly, single crystal silicon (100) wafer (p-type, Boron-doped, resistivity of 8-25 Ω·cm) was treated at 80ºC for 1 hour in piranha solution that contained 3:1 (v/v) concentrated

H_2SO_4:30% H_2O_2, and rinsed with deionized water to remove contamination from organic grease. Subsequently, the silicon substrates were sonicated in 5:1:1 $H_2O/NH_4OH/H_2O_2$ for 60 minutes and washed with a large amount of deionized water. After treatment, the substrates became very hydrophilic due to the production of hydroxyl groups. The treated substrates were stored in deionized water and used within one week. In order to form nanosphere mask, a droplet of polystyrene nanospheres solution at original concentration were dropped onto a cleaned silicon substrate and allowed to dry, forming a monolayer in a close-packed hexagonal structure. The nanosphere monolayer coated substrates were then treated by oxygen plasma for various times ranging from 5 to 15 minutes. The purpose of oxygen plasma treatment was to reduce the particle size and make a mask for metal deposition. A thermal evaporator (Denton) was used to deposit a 10 nm gold film onto the substrates in vacuum at a pressure lower than 5.0×10^{-6} Torr. Following gold deposition, the polystyrene nanospheres were removed by dissolution in chloroform ($CHCl_3$) to create an ordered array of nanoholes, where the diameters of holes were determined by the diameter-reduced polystyrene nanospheres. At last, silicon under gold was etched in a mixture of deionized water, 10 wt% HF and 1.5 wt% H_2O_2, and then rinsed with ethanol and deionized water for 20 seconds, respectively.

4.2.4 Surface modification of phase change nanoparticles

The surface modification of nanoparticles was carried out as following. The as-prepared indium nanoparticles were put into an oven and kept at 110ºC in ambient condition for 10 minutes, which produced a thin oxide layer around the nanoparticles. The nanoparticles with thin oxide films were modified with amine-terminated monolayer by immersing in a 5% APTES/toluene solution for 1 hour at room temperature, followed by washing with toluene and

DMSO for three times, respectively. The APTES modified nanoparticles were resuspended in a DMSO solution containing DSS for 1 hour. After removing excess DSS by centrifugation and washing by a buffer solution (PBS, pH 7.4) for three times, the nanoparticles were incubated in 500 µl of 60 µM thrombin aptamer in PBS for another 2 hours.

4.2.5 Surface modification of substrates

The aluminum surfaces and filter paper were modified with APTES, where the surfaces were kept in a sealed vial containing a ~50 µl droplet of APTES, and heated up to 110 ºC for 1 hour. Then the amine-terminated surfaces were immersed in a DMSO solution containing DSS for 1 hour. After washing with DMSO and PBS, the modified aluminum surface or filter paper was immersed in a PBS solution containing certain amount of thrombin aptamer for 2 hours. Unbounded oligonucleotides were removed by rinsing thoroughly with PBS (pH 7.4). The aptamer-modified surfaces were incubated with thrombin at different concentrations in a buffer solution, containing 34 mM Tris-HCl (pH of 7.4), 233 mM NaCl, 8.5 mM KCl, 1.7 mM $CaCl_2$, 1.7 mM $MgCl_2$, 8.5% glycerol (v/v), for 1 hour. After washing by PBS, the surface with immobilized thrombin was exposed to aptamer functionalized nanoparticles in PBS for another 1 hour. The substrates were then rinsed thoroughly with PBS and dried for thermal detection.

The silicon nanostructured substrates were first treated by a mixture of H_2SO_4 and H_2O_2 at volume ratio 3:1 for 1hour at 80ºC washed thoroughly with deionized water and modified with amine-terminated monolayer by incubating in 5% APTES ethanol solution for 1 hour. After rinsing with ethanol and DMSO, the amine-terminated silicon substrates were immersed in a DMSO solution containing DSS for 1 hour. The substrates were then washed with DMSO and

PBS for three times, respectively, and incubated with thrombin aptamer in PBS for 2 hours. In the next, the surface with immobilized thrombin was exposed to aptamer functionalized nanoparticles in PBS for another 1 hour. The substrates were then rinsed thoroughly with PBS and dried for thermal detection.

4.2.6 Thermal readout of thrombin-immobilized nanoparticles

A PerkinElmer DSC (DSC 7) was used to measure the melting temperatures and fusion enthalpies of phase change nanoparticles. For nanoparticle characterization, 10 mg of nanoparticles was sealed in an aluminum pan and the DSC test was carried out from 50 to 200°C at a ramp rate of 10°C per minute. An empty aluminum pan was used as reference to derive the difference in heat flows of sample and reference. For thrombin detection, the aluminum surface was also modified with a monolayer of amine-terminated molecules using APTES. In order to capture thrombin from solution, thrombin aptamer was immobilized onto amine-terminated aluminum surfaces using DSS as cross-linker. Once thrombin was immobilized, the aluminum surface was exposed to aptamer functionalized phase change nanoparticles in PBS for 1 hour. After rinsed with PBS and dried, the substrates were ready for thermal readout.

4.3 Results and discussion

4.3.1 Nanostructured Si surface

The procedure for the fabrication of silicon nanopillar arrays has been described in experimental section of 2.3. The morphologies of the resulting structures created on silicon substrates are studied by a Zeiss Ultra 55 scanning electron microscope (SEM) at accelerating voltage of 10 kV. Figure 4.2A shows a SEM image of closed-packed polystyrene nanospheres

62

monolayer coated on a clean silicon substrate. Figure 4.2B shows a SEM image of polystyrene nanospheres with reduced diameter of 350 nm after etching by oxygen plasma for 5 minutes. Figure 4.2C shows an ordered array of nanoholes on the silicon surface after evaporating 10 nm gold thin films and removing the polystyrene nanospheres. Figure 4.2D shows a SEM image of silicon nanopillar arrays, where the size of the nanopillars and the center-to-center distances between them can be controlled by selecting appropriate sizes of nanospheres, and etching condition. Some nanopillars stick together, probably because the attractive capillary force during drying between nanopillars is larger than that needed to bend nanopillars.
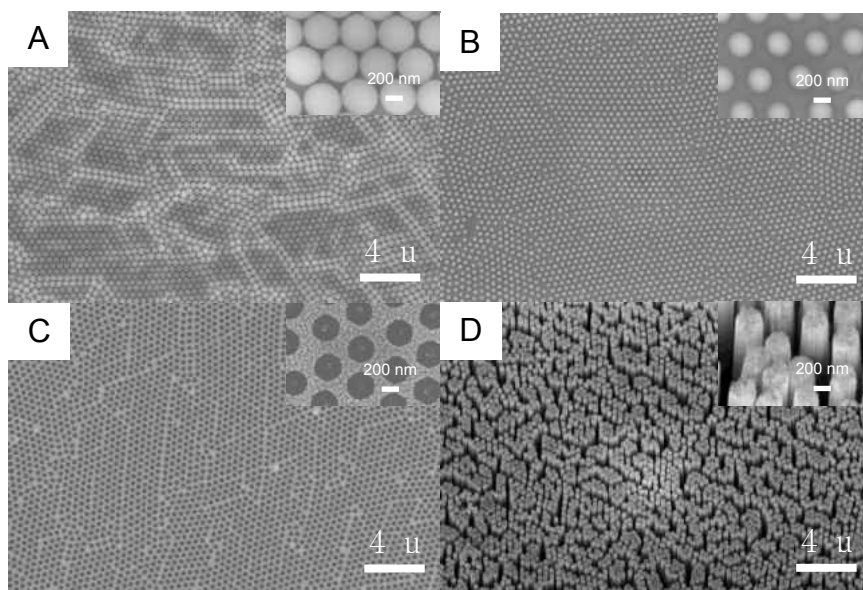
Figure 4.2 SEM image of close-packed nanospheres on clean silicon surface before (A) and after etching in oxygen plasma for 5 minutes (B); an ordered array of gold nanoholes (C); cross-section SEM image of silicon nanopillars after 10 minutes' etching (D).

4.3.2 Thrombin detection in buffer solutions on Al and filter-paper surfaces

Buffer solutions containing thrombin at concentrations from 220 to 22 nM are used as standard samples. The aptamer functionalized surfaces are immersed in the buffers for 2 hour to capture thrombin. After washing the surface, aptamer functionalized nanoparticles are attached onto thrombin immobilized surfaces in buffer solution. After reacting for another 1 hour, the aluminum surface is taken out of the solution, washed by PBS, dried and tested by DSC. The melting peaks of phase change nanoparticles immobilized on the substrate through aptamer-thrombin interaction are used for the qualitative and quantitative detections of thrombin. Figure 4.3A shows melting peaks of indium nanoparticles, where the curves from top to bottom correspond to the concentrations of thrombin from 220 to 22 nM, respectively. The peak areas should be related to the mass of nanoparticles or the mole number of thrombin immobilized on the substrates, and can be derived by integrating heat flow over the melting range. Figure 4.3B shows the relation between the peak area and the concentration of thrombin.
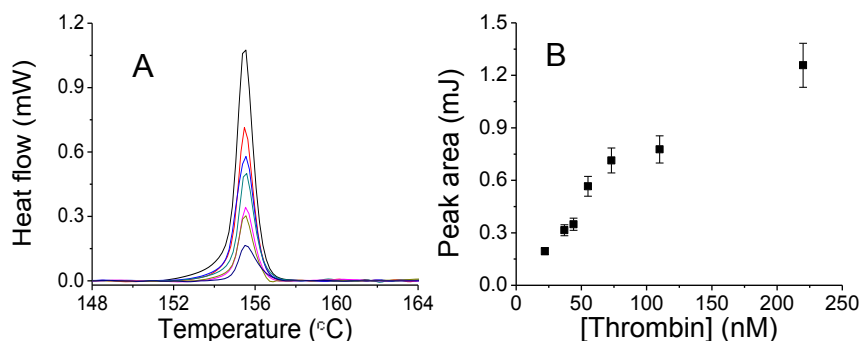
Figure 4.3 DSC curves of indium nanoparticles immobilized on aluminum through thrombin in buffer solution (A); the relation between thrombin concentrations and melting peak area of indium nanoparticles (B).

Similarly, filter paper can also be modified and used to detect thrombin. Figure 4.4C shows the DSC melting peak of indium nanoparticles immobilized on filter paper, where the curves from top to bottom correspond to thrombin concentrations from 220 to 22 nM, respectively. The peak area reduces as thrombin concentration drops. Figure 4.4D shows the relation between the peak area and the thrombin concentration. The detection sensitivity (22 nM) is comparable or better than those of most existing techniques.[150]

Figure 4.4 DSC curves of indium nanoparticles captured on filter paper by thrombin at different concentrations in buffer solutions (C), where the concentration of thrombin is from 220 to 22 nM; the relation between thrombin concentrations and melting peak area of indium nanoparticles (D).

4.3.3 Thrombin detection in buffer solutions on nanostructured Si surfaces

The detection sensitivity is dependent on the mass and the latent heat of fusion of phase change nanoparticles immobilized on substrates. By increasing the surface area of the substrate, the sensitivity for detection can be enhanced. Silicon surfaces with vertically-aligned high-aspect-ratio nanopillars have been used for thermal detection. The silicon nanopillars are modified by APTES and activated by DSS. After reacting with aptamer for 2 hours, the substrate is immersed in a buffer solution containing different concentrations of thrombin. The aptamer

functionalized surface is incubated with aptamer-functionalized nanoparticles in a buffer solution containing thrombin for 1 hour. Figure 4.5A shows an EDX spectrum of indium nanoparticles, confirming immobilization of nanoparticles on silicon nanopillars. The silicon nanopillars have been regenerated and re-used for detection, where the immobilized nanoparticles had been removed by annealing at 500°C for 10 minutes and immersing in piranha solution for 30 minutes. The nanoparticles can be immobilized onto the clean substrates again using the same procedure. This process has been repeated three times without affecting detection sensitivity. Figure 4.5B shows the melting peak of indium nanoparticles immobilized on the nanostructured silicon surface, where the curves correspond to the thrombin concentrations from 220 to 22 nM. The relation between the melting peak area and thrombin concentration is plotted in Figure 4.5C, where the peak area is proportional to the concentration of thrombin in a certain range. The surface area of a substrate with an array of nanopillars (200 nm in diameter, and 2 μm in height) is about 10 times larger that that of a flat surface with the same size. Figure 4.5D shows the normalized sensitivity (peak area per mm^2) at different thrombin concentrations, where the sensitivity of the nanostructured silicon surface is enhanced by four times at thrombin concentration of 55 nM.
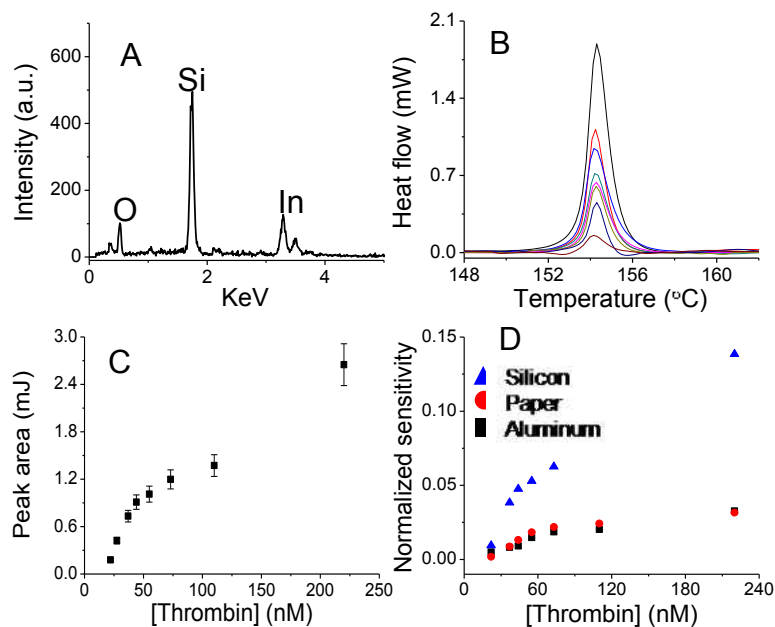
Figure 4.5 EDX spectrum of silicon nanopillars after (A) immobilizing indium nanoparticles; DSC curves of indium nanoparticles captured on silicon nanopillars by thrombin at different concentration in buffer solution (B), where the concentration of thrombin is from 220 to 22 nM; the relation between thrombin concentration and melting peak area of indium nanoparticles (C); normalized sensitivity (melting peak area per mm^2) versus the concentration of thrombin (D).

4.3.4 Thrombin detection in calf serum

Fetal calf serum is the portion of plasma remaining after blood coagulation, during which process plasma protein fibrinogen is converted into fibrin and remains behind in clot, making the detection of thrombin in plasma or blood clinically relevant. The melting temperature of indium nanoparticles made in our experiment is higher than the coexisting specifies in calf serum, thus the thermal readout will not be interfered by species contained in calf serum. Thrombin is added at certain concentration (220, 110, 55 and 22 nM) into a buffered saline containing 10% calf serum, and detected using the same method. Figure 4.6A shows the melting peaks of indium

nanoparticles that are immobilized on aluminum surfaces after thrombin detection, where the curves from top to bottom are collected at thrombin concentrations of 220, 110, 55, and 22 nM, respectively. Although the temperature scan range is from 50 to 200ºC, only the thermal behavior in the range from 148 to 164ºC is shown for display clarity. Figure 4.6B shows the relation between the peak area and the concentration of thrombin detected on aluminum surfaces. Figure 4.6C shows DSC curves of indium nanoparticles collected at different concentrations of thrombin on nanostructured silicon surfaces. Figure 4.6D also shows a relation between the measured peak area and the concentration of thrombin. The peak areas measured at different concentration of thrombin in buffer have been compared with those in calf serum. Similar trends are observed when the same testing conditions are used, but the peak areas measured from serum solution are ~50% lower than that from buffer solution. In contrast to buffer solutions that have defined composition, serum contains abundant proteins that can affect detection of thrombin through specific interaction or non-specific adsorption, thus causing heat flow reduction.
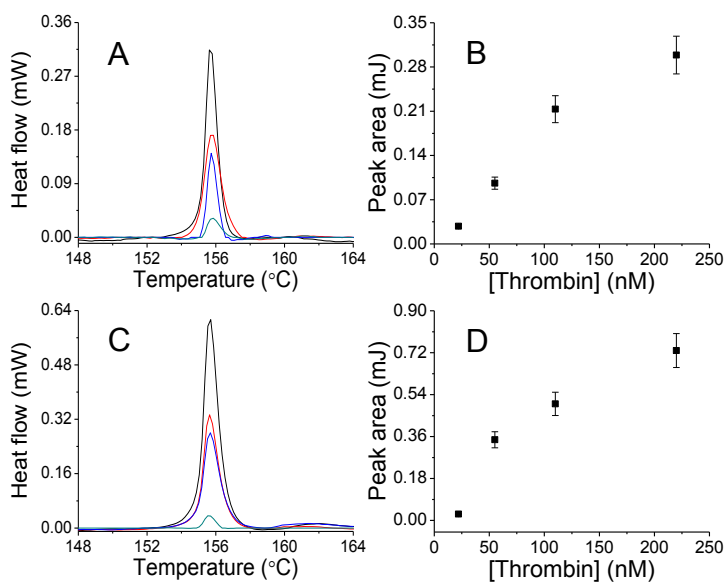
Figure 4.6 DSC curves of indium nanoparticles immobilized on aluminum surface after detecting thrombin at different concentration in calf serum buffered saline (A); the relation between th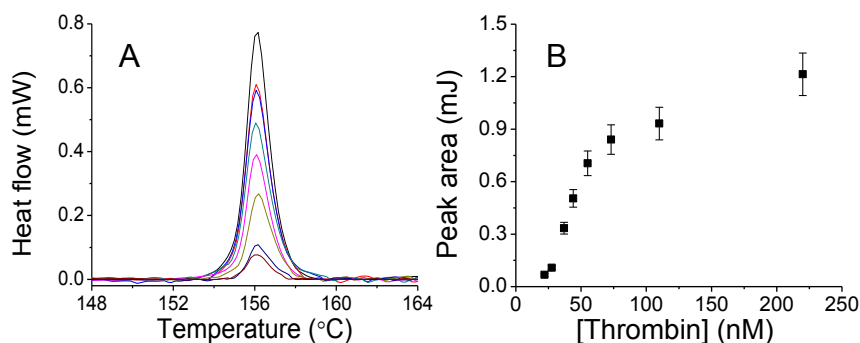rombin concentrations and peak areas of indium nanoparticles (B); DSC curves of indium nanoparticles captured on silicon nanopillars by thrombin at different concentrations in buffer solutions (C); the relation between thrombin concentrations and peak areas of nanoparticles (D).

4.4 Conclusions

We have developed a scanning calorimetric method for highly sensitive detection of thrombin by using RNA aptamer-functionalized phase change nanoparticles. The presence of thrombin in solution leads to attachment of nanoparticles on a substrate modified with the same aptamer. The phase changes of nanoparticles from solid to liquid are detected by measuring heat flow after immobilization. The position and area of melting peak reflect the existence and concentration of thrombin. High aspect ratio silicon nanopillars have shown to enhance the detection sensitivity by four times at thrombin concentration of 55 nM. The detection sensitivity is comparable or better than those of most existing techniques. The thermal detection can be performed in serum because thermal readout is immune to colored species. This new technique provides a highly sensitive, specific and low-cost method for bio-detection using aptamer based sandwich protein assay.

REFERENCES

1. Hanahan, D.; Weinberg, R. A., The hallmarks of cancer. *Cell* **2000**, 100, 57.

2. Menon, U.; Jacobs, I. J., Recent developments in ovarian cancer screening. *Curr. Opin. Obstet. Gynecol.* **2000**, 12, 39.

3. Kumar, B.; Yadav, P. R.; Goel, H. C.; Rizvil, M. M., Recent developments in cancer therapy by the use of nanotechnology. *Dig. J. nanomater. Bios.* **2009**, 4, 1.

4. Liotta, L.; Petricoin, E., Molecular profiling of human cancer. *Nat. Rev. Genet.* **2000**, 1, 48.

5. Fleiter, T.; Merkle, E. M.; Aschoff, A. J.; Lang, G.; Stein, M.; Gorich, J.; Liewald, F.; Rilinger, N.; Sokiranski, R., Comparison of real-time virtual and fiberoptic bronchoscopy in patients with bronchial carcinoma: opportunities and limitations. *Am. J. Roentgenol.* **1997**, 169, 1591.

6. Makarov, D. V.; Loeb, S.; Getzenberg, R. H.; Partin, A. W., Biomarkers for prostate cancer. *Annu. Rev. Med.* **2009**, 60, 139.

7. Bartlett, J. M.; Stirling, D., A short history of the polymerase chain reaction. In *PCR protocols*, 2003; Vol. 226, pp 3.

8. Bernard, P. S.; Wittwer, C. T., Real-time PCR technology for cancer diagnostics. *Clin. Chem.* **2002**, 48, 1178.

9. Hoshi, S.; Kobayashi, S.; Takahashi, T.; Suzuki, K. I.; Kawamura, S.; Satoh, M.; Chiba, Y.; Orikasa, S., Enzyme-linked immunosorbent assay detection of prostate-specific antigen messenger ribonucleic acid in prostate cancer. *Urology* **1999**, 53, 228.

10. Guo, Q. M., DNA microarray and cancer. *Curr. Opin. Oncol.* **2003**, 15, 36.

11. Saiki, R. K.; Scharf, S.; Faloona, F.; Mullis, K. B.; Horn, G. T.; Erlich, H. A.; Arnheim, N., Enzymatic amplification of beta-globin genomic sequences and restriction site analysis for diagnosis of sickle cell anemia. *Science* **1985**, 230, 1350.

12. Saiki, R. K.; Gelfand, D. H.; Stoffel, S.; Scharf, S. J.; Higuchi, R.; Horn, G. T.; Mullis, K. B.; Erlich, H. A., Primer-directed enzymatic amplification of DNA with a thermostable DNA polymerase. *Science* **1988**, 239, 487.

13. Ozkumur, E.; Ahn, S.; Yalcin, A.; Lopez, C. A.; Cevik, E.; Irani, R. J.; DeLisi, C.; Chiari, M.; Unlu, M. S., Label-free microarray imaging for direct detection of DNA hybridization and single-nucleotide mismatches. *Biosens. Bioelectron.* 25, 1789.

14. Konry, T.; Hayman, R. B.; Walt, D. R., Microsphere-based rolling circle amplification microarray for the detection of DNA and proteins in a single assay. *Anal. Chem.* **2009**, 81, 5777.

15. Watanabe, T.; Kobunai, T.; Toda, E.; Kanazawa, T.; Kazama, Y.; Tanaka, J.; Tanaka, T.; Yamamoto, Y.; Hata, K.; Kojima, T.; Yokoyama, T.; Konishi, T.; Okayama, Y.; Sugimoto, Y.; Oka, T.; Sasaki, S.; Ajioka, Y.; Muto, T.; Nagawa, H., Gene expression signature and the prediction of ulcerative colitis-associated colorectal cancer by DNA microarray. *Clin. Cancer. Res.* **2007**, 13, 415.

16. Santra, S.; Zhang, P.; Wang, K.; Tapec, R.; Tan, W., Conjugation of biomolecules with luminophore-doped silica nanoparticles for photostable biomarkers. *Anal. Chem.* **2001**, 73, 4988.

17. Resch-Genger, U.; Grabolle, M.; Cavaliere-Jaricot, S.; Nitschke, R.; Nann, T., Quantum dots versus organic dyes as fluorescent labels. *Nat Meth* **2008**, 5, 763.

18. Gao, X.; Cui, Y.; Levenson, R. M.; Chung, L. W. K.; Nie, S., In vivo cancer targeting and imaging with semiconductor quantum dots. *Nat. Biotechnol.* **2004**, 22, 969.

71

19. Wu, X.; Liu, H.; Liu, J.; Haley, K. N.; Treadway, J. A.; Larson, J. P.; Ge, N.; Peale, F.; Bruchez, M. P., Immunofluorescent labeling of cancer marker Her2 and other cellular targets with semiconductor quantum dots. *Nat. Biotechnol.* **2003**, 21, 41.

20. Bruchez, M., Jr.; Moronne, M.; Gin, P.; Weiss, S.; Alivisatos, A. P., Semiconductor nanocrystals as fluorescent biological labels. *Science* **1998**, 281, 2013.

21. Chan, W. C. W.; Maxwell, D. J.; Gao, X.; Bailey, R. E.; Han, M.; Nie, S., Luminescent quantum dots for multiplexed biological detection and imaging. *Curr. Opin. Biotechnol.* **2002**, 13, 40.

22. Wabuyele, M. B.; Vo-Dinh, T., Detection of human immunodeficiency virus type 1 DNA sequence using plasmonics nanoprobes. *Anal. Chem.* **2005**, 77, 7810.

23. Haes, A. J.; Van Duyne, R. P., A nanoscale optical biosensor: sensitivity and selectivity of an approach based on the localized surface plasmon resonance spectroscopy of triangular silver nanoparticles. *J. Am. Chem. Soc.* **2002**, 124, 10596.

24. Haes, A. J.; Hall, W. P.; Chang, L.; Klein, W. L.; Van Duyne, R. P., A localized surface plasmon resonance biosensor: first steps toward an assay for Alzheimer's disease. *Nano Lett.* **2004**, 4, 1029.

25. Backmann, N.; Zahnd, C.; Huber, F.; Bietsch, A.; Pluckthun, A.; Lang, H.-P.; Guntherodt, H.-J.; Hegner, M.; Gerber, C., A label-free immunosensor array using single-chain antibody fragments. *Proc. Natl. Acad. Sci. USA* **2005**, 102, 14587.

26. Schultz, S.; Smith, D. R.; Mock, J. J.; Schultz, D. A., Single-target molecule detection with nonbleaching multicolor optical immunolabels. *Proc. Natl. Acad. Sci. USA* **2000**, 97, 996.

27. Mie, G., Contributions to the optics of turbid media particularly of colloidal metal solutions. *Ann. Phys.* **1908**, 330, 377.

28. Cai, H.; Xu, Y.; Zhu, N.; He, P.; Fang, Y., An electrochemical DNA hybridization detection assay based on a silver nanoparticle label. *Analyst* **2002**, 127, 803.

29. Wang, J.; Liu, G.; Merkoçi, A., Particle-based detection of DNA hybridization using electrochemical stripping measurements of an iron tracer. *Anal. Chim. Acta* **2003**, 482, 149.

30. Dequaire, M.; Degrand, C.; Limoges, B. t., An electrochemical metalloimmunoassay based on a colloidal gold label. *Anal. Chem.* **2000**, 72, 5521.

31. Authier, L.; Grossiord, C.; Brossier, P.; Limoges, B., Gold nanoparticle-based quantitative electrochemical detection of amplified human cytomegalovirus DNA using disposable microband electrodes. *Anal. Chem.* **2001**, 73, 4450.

32. Okuno, J.; Maehashi, K.; Kerman, K.; Takamura, Y.; Matsumoto, K.; Tamiya, E., Label-free immunosensor for prostate-specific antigen based on single-walled carbon nanotube array-modified microelectrodes. *Biosens. Bioelectron.* **2007**, 22, 2377.

33. Bai, Y.; Sun, Y.; Sun, C., Pt-Pb nanowire array electrode for enzyme-free glucose detection. *Biosens. Bioelectron.* **2008**, 24, 579.

34. Erich, C. W.; Michael, P. Z.; Frédéric, F.; Benjamin, J. M.; Koji, I.; John, C. H.; Reginald, M. P., Metal nanowire arrays by electrodeposition. *Chem. Phys. Chem.* **2003**, 4, 131.

35. Bangar, M. A.; Ramanathan, K.; Yun, M.; Lee, C.; Hangarter, C.; Myung, N. V., Controlled growth of a single palladium nanowire between microfabricated electrodes. *Chem. Mater.* **2004**, 16, 4955.

36. Grossman, H. L.; Myers, W. R.; Vreeland, V. J.; Bruehl, R.; Alper, M. D.; Bertozzi, C. R.; Clarke, J., Detection of bacteria in suspension by using a superconducting quantum interference device. *Proc. Natl. Acad. Sci. USA* **2004**, 101, 129.

37. Balasubramanian, S.; Yuanpeng, L.; Ying, J.; YunHao, X.; Xiaofeng, Y.; Chengguo, X.; Jian-Ping, W., A Detection system based on giant magnetoresistive sensors and high-moment magnetic nanoparticles demonstrates zeptomole sensitivity: potential for personalized medicine. *Angew. Chem. Int. Ed.* **2009**, 48, 2764.

38. Mihajlovic, G.; Xiong, P.; von Molnar, S.; Field, M.; Sullivan, G. J.; Ohtani, K.; Ohno, H., Submicrometer hall sensors for superparamagnetic nanoparticle detection. *IEEE Trans. Magn.* **2007**, 43, 2400.

39. Patolsky, F.; Zheng, G.; Lieber, C. M., Nanowire-based biosensors. *Anal. Chem.* **2006**, 78, 4260.

40. Lu, Y.; Ji, H.-F., Electric field-directed assembly of gold and platinum nanowires from an electrolysis process. *Electrochem. Commun.* **2008**, 10, 222.

41. Raychaudhuri, S.; Dayeh, S. A.; Wang, D.; Yu, E. T., Precise semiconductor nanowire placement through dielectrophoresis. *Nano Lett.* **2009**, 9, 2260.

42. Lee, S. H.; Lee, H. J.; Oh, D.; Lee, S. W.; Goto, H.; Buckmaster, R.; Yasukawa, T.; Matsue, T.; Hong, S.-K.; Ko; Cho, M.-W.; Yao, T., Control of the ZnO nanowires nucleation site using microfluidic channels. *J. Phys. Chem. B* **2006**, 110, 3856.

43. Conache, G.; et al., AFM-based manipulation of InAs nanowires. *J. Phys: Conf. Ser.* **2008**, 100, 052051.

44. Hansen, K. M.; Ji, H.-F.; Wu, G.; Datar, R.; Cote, R.; Majumdar, A.; Thundat, T., Cantilever-based optical deflection assay for discrimination of DNA single-nucleotide mismatches. *Anal. Chem.* **2001**, 73, 1567.

45. Yan, X.; Xu, X. K.; Ji, H.-F., Glucose oxidase multilayer modified microcantilevers for glucose measurement. *Anal. Chem.* **2005**, 77, 6197.

46. Pera, I.; Fritz, J. r., Sensing lipid bilayer formation and expansion with a microfabricated cantilever array. *Langmuir* **2006**, 23, 1543.

47. Arntz, Y.; Seelig, J. D.; Lang, H. P.; Zhang, J.; Hunziker, P.; Ramseyer, J. P.; Meyer, E.; Hegner, M.; Gerber, C., Label-free protein assay based on a nanomechanical cantilever array. *Nanotechnology* **2003**, 14, 86.

48. Wu, G.; Datar, R. H.; Hansen, K. M.; Thundat, T.; Cote, R. J.; Majumdar, A., Bioassay of prostate-specific antigen (PSA) using microcantilevers. *Nat. Biotechnol.* **2001**, 19, 856.

49. Wu, G.; Ji, H.; Hansen, K.; Thundat, T.; Datar, R.; Cote, R.; Hagan, M. F.; Chakraborty, A. K.; Majumdar, A., Origin of nanomechanical cantilever motion generated from biomolecular interactions. *Proc. Natl. Acad. Sci. USA* **2001**, 98, 1560.

50. Sawyer, C. L., The cancer biomarker problem. *Nature* **2008**, 452, 548.

51. Ferrari, M., Cancer nanotechnology: opportunities and challenges. *Nature Rev. Cancer* **2005**, 5, 161.

52. Jain, K. K., Cancer biomarkers: current issues and future directions. *Curr. Opin. Mol. Ther.* **2007**, 9, 563.

53. Danila, D. C.; Heller, G.; Gignac, G. A.; Gonzalez-Espinoza, R.; Anand, A.; Tanaka, E.; Lilja, H.; Schwartz, L.; Larson, S.; Fleisher, M.; Scher, H. I., Circulating tumor cell number and prognosis in progressive castration-resistant prostate cancer. *Clin. Cancer Res.* **2007**, 13, 7053.

54. Zheng, S.; Lin, H.; Liu, J. Q.; Balic, M.; Datar, R.; Cote, R. J.; Tai, Y.-C., Membrane microfilter device for selective capture, electrolysis and genomic analysis of human circulating tumor cells. *J. Chromatogr. A* **2007**, 1162, 154.

55. Nagrath, S.; Sequist, L. V.; Maheswaran, S.; Bell, D. W.; Irimia, D.; Ulkus, L.; Smith, M. R.; Kwak, E. L.; Digumarthy, S.; Muzikansky, A.; Ryan, P.; Balis, U. J.; Tompkins, G.; Haber, D. A.; Toner, M., Isolation of rare circulating tumor cells in cancer patients by microchip technology. *Nature* **2007**, 450, 1235.

56. Maraldo, D.; Garcia, F. U.; Mutharasan, R., Method for quantification of a prostate cancer biomarker in urine without sample preparation. *Anal. Chem.* **2007**, 79, 7683.

57. Paul, B.; Dhir, R.; Landsittel, D.; Hitchens, M. R.; Getzenberg, R. H., Detection of prostate cancer with a blood-based assay for early prostate cancer antigen. *Cancer Res.* **2005**, 15, 4097.

58. Acharya, G.; Chang, C.-L.; Doorneweerd, D. D.; Vlashi, E.; Henne, W. A.; Hartmann, L. C.; Low, P. S.; Savran, C. A., Immunomagnetic diffractometry for detection of diagnostic serum markers. *J. Am. Chem. Soc.* **2007**, 129, 15824.

59. Bertram, H. C.; Eggers, N.; Eller, N., Potential of human saliva for nuclear magnetic resonance-based metabolomics and for health-related biomarker identification. *Anal. Chem.* **2009**, 81, 9188.

60. Xiang, F.; Anderson, G. A.; Veenstra, T. D.; Lipton, M. S.; Smith, R. D., Characterization of microorganisms and biomarker development from global ESI-MS/MS analyses of cell lysates. *Anal. Chem.* **2000**, 72, 2475.

61. Lazar, I. M.; Trisiripisal, P.; Sarvaiya, H. A., Microfluidic liquid chromatography system for proteomic applications and biomarker screening. *Anal. Chem.* **2006**, 78, 5513.

62. Yang, W.; Sun, X.; Wang, H.-Y.; Woolley, A. T., Integrated microfluidic device for serum biomarker quantitation using either standard addition or a calibration curve. *Anal. Chem.* **2009**, 81, 8230.

63. Griep, M.; Whitney, S.; Nelson, M.; Viljoen, H., DNA polymerase chain reaction: a model of error frequencies and extension rates. *AIChE J.* **2006**, 52, 384.

64. Pita, M.; Cui, L.; Gaikwad, R. M.; Katz, E.; Sokolov, I., High sensitivity molecular detection with enzyme-linked immuno-sorbent assay (ELISA)-type immunosensing. *Nanotechnology* **2008**, 19, 375502.

65. Walt, D. R., Miniature analytical methods for medical diagnostics *Science* **2005**, 308, 217.

66. Mani, V.; Chikkaveeraiah, B. V.; Patel, V.; Gutkind, J. S.; Rusling, J. F., Ultrasensitive immunosensor for cancer biomarker proteins using gold nanoparticle film electrodes and multienzyme-particle amplification. *ACS Nano* **2009**, 3, 585.

67. Huang, X. H.; Jain, P. K.; El-Sayed, I. H.; El-Sayed, M. A., Gold nanoparticles: interesting optical properties and recent applications in cancer diagnostic and therapy. *Nanomed.* **2007**, 2, 681.

68. White, K. A.; Rosi, N. L., Gold nanoparticle-based assays for the detection of biologically relevant molecules. *Nanomedicine* **2008**, 3, 543.

69. Alivisatos, P., The use of nanocrystals in biological detection. *Nature Biotechnol.* **2004**, 22, 47.

70. Nam, J. M.; Thaxton, C. S.; Mirkin, C. A., Nanoparticle-based bio-bar codes for the ultrasensitive detection of proteins. *Science* **2003**, 301, 1884.

71. Park, S.-J.; Taton, T. A.; Mirkin, C. A., Array-based electrical detection of DNA with nanoparticle probes. *Science* **2002**, 295, 1503.

72. Wang, J.; Liu, G.; Engelhard, M. H.; Lin, Y., Sensitive immunoassay of a biomarker tumor necrosis factor-α Based on poly(guanine)-functionalized silica nanoparticle label. *Anal. Chem.* **2006**, 78, 6974.

73. Radomska, A.; Eodenszac, E.; Glab, S.; Koncki, R., Creatinine biosensor based on ammonium ion selective electrode and its application in flow-injection analysis. *Talanta* **2004**, 64, 603.

74. Hutton, L.; Newton, M. E.; Unwin, P. R.; Macpherson, J. V., Amperometric oxygen sensor based on a platinum nanoparticle-modified polycrystalline boron doped diamond disk electrode. *Anal. Chem.* **2009**, 81, 1023.

75. Josephson, L.; Perez, J. M.; Weissleder, R., Magnetic nanosensors for the detection of oligonucleotide sequences. *Angew. Chem. Int. Ed.* **2001**, 40, 3204.

76. Kitagawa, D.; Kajiho, H.; Negishi, T.; Ura, S.; Watanabe, T.; Wada, T.; Ichijo, H.; Katada, T.; Nishina, H., Release of RASSF1C from the nucleus by Daxx degradation links DNA damage and SAPK/JNK activation *EMBO J.* **2006**, 25, 3286.

77. Meyer, H. E.; Stuhler, K., High-performance proteomics as a tool in biomarker discovery. *Proteomics.* **2007**, 7, 18.

78. Collins, J. M., Imaging and other biomarkers in early clinical studies: one step at a time or re-engineering drug development? *J. Clin. Oncol.* **2005**, 23, 5417.

79. Wei, F.; Patel, P.; Liao, W.; Chaudhry, K.; Zhang, L.; Arellano-Garcia, M.; Hu, S.; Elashoff, D.; Zhou, H.; Shukla, S.; Shah, F.; Ho, C.-M.; Wong, D. T., Electrochemical sensor for multiplex biomarkers detection. *Clin. Cancer Res.* **2009**, 15, 4446.

80. Kozak, K. R.; Su, F.; Whitelegge, J. P.; Faull, K.; Reddy, S.; Farisa-Eisner, R., Characterization of serum biomarkers for detection of early stage ovarian cancer. *Proteomics.* **2005**, 5, 4589.

81. Mohamed, M. B.; Wang, Z. L.; El-Sayed, M. A., Temperature-dependent size-controlled nucleation and growth of gold nanoclusters. *J. Phys. Chem. A* **1999**, 103, 10255.

82. Dippel, M.; Maier, A.; Gimple, V.; Wider, H.; Evenson, W. E.; Rasera, R. L.; Schatz, G., Size-dependent melting of self-assembled indium nanostructures. *Phys. Rev. Lett.* **2001**, 87, 095505.

83. Jain, K. K., Cancer biomarkers: current issues and future directions. *Curr. Opin. Mol. Ther.* **2007**, 9, 563.

84. Diamandis, E. P., Analysis of serum proteomic patterns for early cancer diagnosis: Drawing attention to potential problems. *J. Natl. Cancer Inst.* **2004**, 96, 353.

85. Sawyers, C. L., The cancer biomarker problem. *Nature* **2008**, 452, 548.

86. Pita, M.; Cui, L.; Gaikwad, R. M.; Katz, E.; Sokolov, I., High sensitivity molecular detection with enzyme-linked immuno-sorbent assay (ELISA)-type immunosensing. *Nanotechnology* **2008**, 19.

87. Nam, J.-M.; Thaxton, C. S.; Mirkin, C. A., Nanoparticle-based bio-bar codes for the ultrasensitive detection of proteins. *Science* **2003**, 301, 1884.

88. Ferrari, M., Cancer nanotechnology: opportunities and challenges. *Nat. Rev. Cancer* **2005**, 5, 161.

89. Bao, Y. P.; Wei, T.-F.; Lefebvre, P. A.; An, H.; He, L.; Kunkel, G. T.; Muller, U. R., Detection of protein analytes via nanoparticle-based bio bar code technology. *Anal. Chem.* **2006**, 78, 2055.

90. Rosi, N. L.; Mirkin, C. A., Nanostructures in biodiagnostics. *Chem. Rev.* **2005**, 105, 1547.

91. Alivisatos, P., The use of nanocrystals in biological detection. *Nat Biotech* **2004**, 22, 47.

92. Han, M.; Gao, X.; Su, J. Z.; Nie, S., Quantum-dot-tagged microbeads for multiplexed optical coding of biomolecules. *Nat Biotech* **2001**, 19, 631.

93. Zimmer, J. P.; Kim, S.-W.; Ohnishi, S.; Tanaka, E.; Frangioni, J. V.; Bawendi, M. G., Size series of small Indium arsenide-zinc selenide core-shell nanocrystals and their application to in vivo imaging. *J. Am. Chem. Soc.* **2006**, 128, 2526.

94. Chan, W. C. W.; Maxwell, D. J.; Gao, X.; Bailey, R. E.; Han, M.; Nie, S., Luminescent quantum dots for multiplexed biological detection and imaging. *Curr. Opin. Biotechnol.* **2002**, 13, 40.

95. Lee, J.; Perez, J. M.; Ralph, W., Magnetic nanosensors for the detection of oligonucleotide sequences. *Angew. Chem. Int. Ed.* **2001**, 40, 3204.

96. So-Jung, P.; Anne , A. L.; Chad , A. M.; Paul , W. B.; Carl , R. K.; Robert , L. L., The electrical properties of gold nanoparticle assemblies linked by DNA. *Angew. Chem. Int. Ed.* **2000**, 39, 3845.

97. Roberts, M. A.; Kelley, S. O., Ultrasensitive detection of enzymatic activity with nanowire electrodes. *J. Am. Chem. Soc* **2007**, 129, 11356.

98. Zheng, G.; Patolsky, F.; Cui, Y.; Wang, W. U.; Lieber, C. M., Multiplexed electrical detection of cancer markers with nanowire sensor arrays. *Nat Biotech* **2005**, 23, 1294.

99. Wang, J.; Xu, D.; Kawde, A.-N.; Polsky, R., Metal nanoparticle-based electrochemical stripping potentiometric detection of DNA hybridization. *Anal. Chem.* **2001**, 73, 5576.

100. Sebra, R. P.; Masters, K. S.; Bowman, C. N.; Anseth, K. S., Surface grafted antibodies: controlled architecture permits enhanced antigen detection. *Langmuir* **2005**, 21, 10907.

101. Zalba, B.; Marín, J. M.; Cabeza, L. F.; Mehling, H., Review on thermal energy storage with phase change: materials, heat transfer analysis and applications. *Appl. Thermal Eng.* **2003**, 23, 251.

102. Wang, F.; Tang, R.; Yu, H.; Gibbons, P. C.; Buhro, W. E., Size- and shape-controlled synthesis of bismuth nanoparticles. *Chem. Mater.* **2008**, 20, 3656.

103. Foos, E. E.; Stroud, R. M.; Berry, A. D.; Snow, A. W.; Armistead, J. P., Synthesis of nanocrystalline bismuth in reverse micelles. *J. Am. Chem. Soc.* **2000**, 122, 7114.

104. Wang, Y.; Xia, Y., Bottom-up and top-down approaches to the synthesis of monodispersed spherical colloids of low melting-point metals. *Nano Lett.* **2004**, 4, 2047.

105. Olson, E. A.; Efremov, M. Y.; Zhang, M.; Zhang, Z.; Allen, L. H., Size-dependent melting of Bi nanoparticles. *J. Appl. Phys.* **2005**, 97, 034304.

106. Jiang, H.; Moon, K.-s.; Dong, H.; Hua, F.; Wong, C. P., Size-dependent melting properties of tin nanoparticles. *Chem. Phys. Lett.* **2006**, 429, 492.

107.   Dippel, M.; Maier, A.; Gimple, V.; Wider, H.; Evenson, W. E.; Rasera, R. L.; Schatz, G., Size-dependent melting of self-assembled indium nanostructures. *Phys. Rev. Lett.* **2001**, 87, 095505.

108.   Ma, L.; Hong, Y.; Ma, Z.; Kaittanis, C.; Perez, J. M.; Su, M., Multiplexed highly sensitive detections of cancer biomarkers in thermal space using encapsulated phase change nanoparticles. *Appl. Phys. Lett.* **2009**, 95, 043701.

109.   Li, T.; Shi, L. L.; Wang, E. K.; Dong, S. J., Silver-ion-mediated DNAzyme switch for the ultrasensitive and selective colorimetric detection of aqueous Ag$^+$ and cysteine. *Chem.-Eur. J.* **2009**, 15, 3347.

110.   He, P. L.; Shen, L.; Cao, Y. H.; Lia, D. F., Ultrasensitive electrochemical detection of proteins by amplification of aptamer-nanoparticle bio bar codes. *Anal. Chem.* **2007**, 79, 8024.

111.   Wang, Y.; Lee, K.; Irudayaraj, J., SERS aptasensor from nanorod-nanoparticle junction for protein detection. *Chem. Commun.* **2010**, 46, 613.

112.   Mir, M.; Vreeke, M.; Katakis, I., Different strategies to develop an electrochemical thrombin aptasensor. *Electrochem. Commun.* **2006**, 8, 505.

113.   Zheng, J.; Cheng, G. F.; He, P. G.; Fang, Y. Z., An aptamer-based assay for thrombin via structure switch based on gold nanoparticles and magnetic nanoparticles. *Talanta* **2010**, 80, 1868.

114.   Chang, H. X.; Tang, L. H.; Wang, Y.; Jiang, J. H.; Li, J. H., Graphene fluorescence resonance energy transfer aptasensor for the thrombin detection. *Anal. Chem.* **2010**, 82, 2341.

115.   Chen, C.-K.; Huang, C.-C.; Chang, H.-T., Label-free colorimetric detection of picomolar thrombin in blood plasma using a gold nanoparticle-based assay. *Biosens. Bioelectron.* **2010**, 25, 1922.

116.   Chung, M. K.; Riby, J.; Li, H.; Iavarone, A. T.; Williams, E. R.; Zheng, Y. X.; Rappaport, S. M., A sandwich enzyme-linked immunosorbent assay for adducts of polycyclic aromatic hydrocarbons with human serum albumin. *Anal. Biochem.* **2010**, 400, 123.

117.   Han, H. J.; Kannan, R. M.; Wang, S. X.; Mao, G. Z.; Kusanovic, J. P.; Romero, R., Multifunctional dendrimer-templated antibody presentation on biosensor surfaces for improved biomarker detection. *Adv. Funct. Mater.* **2010**, 20, 409.

118.   Jia, C. P.; Zhong, X. Q.; Hua, B.; Liu, M. Y.; Jing, F. X.; Lou, X. H.; Yao, S. H.; Xiang, J. Q.; Jin, Q. H.; Zhao, J. L., Nano-ELISA for highly sensitive protein detection. *Biosens. Bioelectron.* **2009**, 24, 2836.

119.   Jokerst, J. V.; Raamanathan, A.; Christodoulides, N.; Floriano, P. N.; Pollard, A. A.; Simmons, G. W.; Wong, J.; Gage, C.; Furmaga, W. B.; Redding, S. W.; McDevitt, J. T., Nano-bio-chips for high performance multiplexed protein detection: Determinations of cancer biomarkers in serum and saliva using quantum dot bioconjugate labels. *Biosens. Bioelectron.* **2009**, 24, 3622.

120.   Ellington, A. D.; Szostak, J. W., In vitro selection of RNA molecules that bind specific ligands. *Nature* **1990**, 346, 818.

121.   Tuerk, C.; Gold, L., Systematic evolution of ligands by exponential enrichment: RNA ligands to bacteriophage T4 DNA polymerase. *Science* **1990**, 249, 505.

122.   Osborne, S. E.; Ellington, A. D., Nucleic acid selection and the challenge of combinatorial chemistry. *Chem. Rev.* **1997**, 97, 349.

123.   Kang, Y.; Feng, K.-J.; Chen, J.-W.; Jiang, J.-H.; Shen, G.-L.; Yu, R.-Q., Electrochemical detection of thrombin by sandwich approach using antibody and aptamer. *Bioelectrochemistry* **2008**, 73, 76.

124.   Pandana, H.; Aschenbach, K. H.; Gomez, R. D., Systematic aptamer-gold nanoparticle colorimetry for protein detection: Thrombin. *IEEE Sens. J.* **2008**, 8, 661.

125.   Wang, Y.; Yang, F.; Yang, X., Colorimetric biosensing of mercury (II) ion using unmodified gold nanoparticle probes and thrombin-binding aptamer. *Biosens Bioelectron* **2010**, 25, 1994.

126.   Zhao, Q.; Lu, X.; Yuan, C.-G.; Li, X.-F.; Le, X. C., Aptamer-linked assay for thrombin using gold nanoparticle amplification and inductively coupled plasma-mass spectrometry detection. *Anal. Chem.* **2009**, 81, 7484.

127.   Hu, J.; Zheng, P. C.; Jiang, J. H.; Shen, G. L.; Yu, R. Q.; Liu, G. K., Electrostatic interaction based approach to thrombin detection by surface-enhanced Raman spectroscopy. *Anal. Chem.* **2009**, 81, 87.

128.   Bizzarri, A. R.; Cannistraro, S., Surface-enhanced Raman spectroscopy combined with atomic force microscopy for ultrasensitive detection of thrombin. *Anal. Biochem.* **2009**, 393, 149.

129.   Wang, Y. L.; Li, D.; Ren, W.; Liu, Z. J.; Dong, S. J.; Wang, E. K., Ultrasensitive colorimetric detection of protein by aptamer - Au nanoparticles conjugates based on a dot-blot assay. *Chem. Commun.* **2008**, 2520.

130.   Lu, Y.; Li, X.; Zhang, L.; Yu, P.; Su, L.; Mao, L., Aptamer-based electrochemical sensors with aptamer-complementary DNA oligonucleotides as probe. *Anal. Chem.* **2008**, 80, 1883.

131.   Zheng, J.; Feng, W.; Lin, L.; Zhang, F.; Cheng, G.; He, P.; Fang, Y., A new amplification strategy for ultrasensitive electrochemical aptasensor with network-like thiocyanuric acid/gold nanoparticles. *Biosens. Bioelectron.* **2007**, 23, 341.

132.   Du, Y.; Chen, C. G.; Yin, J. Y.; Li, B. L.; Zhou, M.; Dong, S. J.; Wang, E. K., Solid-state probe based electrochemical aptasensor for cocaine: A potentially convenient, sensitive, repeatable, and integrated sensing platform for drugs. *Anal. Chem.* **2010**, 82, 1556.

133.   Erdem, A.; Karadeniz, H.; Mayer, G.; Famulok, M.; Caliskan, A., Electrochemical sensing of aptamer-protein interactions using a magnetic particle assay and single-use sensor technology. *Electroanalysis* **2009**, 21, 1278.

134.   Ding, C.; Ge, Y.; Lin, J., Aptamer based electrochemical assay for the determination of thrombin by using the amplification of the nanoparticles. *Biosens. Bioelectron.* **2010**, 25, 1290.

135.   Huang, H. P.; Zhu, J. J., DNA aptamer-based QDs electrochemiluminescence biosensor for the detection of thrombin. *Biosens. Bioelectron.* **2009**, 25, 927.

136.   Li, T.; Wang, E.; Dong, S. J., Chemiluminescence thrombin aptasensor using high-activity DNAzyme as catalytic label. *Chem. Commun.* **2008**, 5520.

137.   Wang, H. X.; Liu, Y.; Liu, C. C.; Huang, J. Y.; Yang, P. Y.; Liu, B. H., Microfluidic chip-based aptasensor for amplified electrochemical detection of human thrombin. *Electrochem. Commun.* **2010**, 12, 258.

138.   Wang, J., Nanomaterial-based electrochemical biosensors. *Analyst* **2005**, 130, 421.

139.   Zhu, N. N.; Zhang, A. P.; Wang, Q. J.; He, P. G.; Fang, Y. Z., Lead sulfide nanoparticle as oligonucleotides labels for electrochemical stripping detection of DNA hybridization. *Electroanalysis* **2004**, 16, 577.

140.   Kanehara, M.; Koike, H.; Yoshinaga, T.; Teranishi, T., Indium tin oxide nanoparticles with compositionally tunable surface plasmon resonance frequencies in the near-IR region. *J. Am. Chem. Soc.* **2009**, 131, 17736.

141.   Panacek, A.; Kvitek, L.; Prucek, R.; Kokar, M.; Vecerova, R.; Pizurova, N.; Sharma, V. K.; Nevecna, T.; Zboril, R., Silver colloid nanoparticles: synthesis, characterization, and their antibacterial activity. *J. Phys. Chem. B* **2006**, 110, 16248.

142.   Tapan, K. S.; Andrey, L. R., Nonspherical noble metal nanoparticles: colloid-chemical synthesis and morphology control. *Adv. Mater.* **2010**, 22, 1781.

143.   Guarise, C.; Pasquato, L.; De Filippis, V.; Scrimin, P., Gold nanoparticles-based protease assay. *Proc. Natl. Acad. Sci. USA* **2006**, 103, 3978.

144.   Li, B. L.; Wang, Y. L.; Wei, H.; Dong, S. J., Amplified electrochemical aptasensor taking AuNPs based sandwich sensing platform as a model. *Biosens. Bioelectron.* **2008**, 23, 965.

145.   Verma, A.; Uzun, O.; Hu, Y.; Hu, Y.; Han, H.-S.; Watson, N.; Chen, S.; Irvine, D. J.; Stellacci, F., Surface-structure-regulated cell-membrane penetration by monolayer-protected nanoparticles. *Nat Mater* **2008**, 7, 588.

146.   Wang, B.; Yu, C., Fluorescence turn-on detection of a protein through the reduced aggregation of a perylene probe. *Angew. Chem. Int. Ed.* **2010**, 49, 1485.

147.   Joseph, W., Nanomaterial-based amplified transduction of biomolecular interactions. *Small* **2005**, 1, 1036.

148.   Taton, T. A.; Mirkin, C. A.; Letsinger, R. L., Scanometric DNA array detection with nanoparticle probes. *Science* **2000**, 289, 1757.

149.   Chang, S. W.; Chuang, V. P.; Boles, S. T.; Ross, C. A.; Thompson, C. V., Densely packed arrays of ultra-high-aspect-ratio silicon nanowires fabricated using block-copolymer lithography and metal-assisted etching. *Adv. Funct. Mater.* **2009**, 19, 2495.

150.   Strehlitz, B.; Nikolaus, N.; Stoltenburg, R., Protein detection with aptamer biosensors. *Sensors* **2008**, 8, 4296.